ISSN 0915-633X

NATIONAL INSTITUTE FOR FUSION SCIENCE

ELMy-H mode as Limit Cycle and Chaotic Oscillations in Tokamak Plasmas

S.-I. Itoh, K. Itoh and A. Fukuyama

(Received – Jun. 3, 1991)

NIFS-96 Jun. 1991

RESEARCH REPORT
NIFS Series

NAGOYA, JAPAN

ELMy-H mode as Limit Cycle and Chaotic Oscillations in Tokamak Plasmas

Sanae-I. Itoh, Kimitaka Itoh,
National Institute for Fusion Science, Nagoya 464-01

Atsushi Fukuyama,
School of Engineering, Okayama University, Okayama 700
Japan

abstract

A model of Edge Localized Modes (ELMs) in tokamaks is presented. A limit cycle solution is found in time-dependent Ginzburg Landau type model equation of L/H transition, which has a hysteresis curve between the plasma gradient and flux. The oscillation of edge density appears near the L/H transition boundary. Spatial structure of the intermediate state (mesophase) is obtained in the edge region. Chaotic oscillation is predicted due to random neutrals and external oscillations.

Keywords: ELMy H-Mode, Edge Plasma, Tokamak, Radial Electric Field, Ion Viscosity, Bifurcation, Limit Cycle, Chaotic Oscillation

§1 Introduction

Edge Localized Modes (ELMs) are known to be regularly observed phenomena characterized by the sudden drop of edge density/temperature with the burst of the particle/heat during the H-phase in tokamak plasmas. When the density/temperature near the plasma edge exceeds a certain threshold value, L- to H-mode transition takes place.[1] In some restricted parameter space of the H phase, ELM activities appear[2]. The ELMs have shown the variety of their appearance. Single giant ELM takes place in an irregular manner in time[2-5], big ELMs or small ELMs or grassy ELMs reveal with a periodic oscillation of H_α bursts[6], and sometimes their mixture appears irregularly.[2-7] Their occurrence is up to now unpredictable in experiments. Among periodic oscillations of ELMs, giant-ELMs and small-ELMs have similar ratio between the period of the ELM and the duration of each burst, which is of the order of 10, and the associated energy loss ratio is also of the order of 10[8]. In grassy-ELMs, a different kind of oscillations has been observed. The period and the duration of the burst have similar values[9]. The grassy ELMs are known to appear near the L/H transition boundary.

The comparison study with critical-β analysis due to MHD ballooning mode[3] has been applied to explain the ELMs. However the analysis has shown that the onset of some ELMs occurs below the threshold value for the β-limit. Resistive MHD analysis[3] on surface peering mode may explain a part of ELMs, however the

assumed current/ pressure profiles are not yet experimentally identified. Furthermore, there remains a question why the structure of associated fluctuation/transport is insensitive to the surface q value and current profile; the period of the Grassy ELMs is left unsolved. A model of ELM as a cyclic oscillation between L and H phases due to impurity accumulation has been proposed[10]. Up to mow, however, the impurity accumulation is considered to be the associated phenomena[3,11].

Based on the bifurcation theory on the L/H transition[12-15], we have proposed a new model theory[16] of grassy-ELMs observed in JFT-2M. The L/H transition has been observed to have a hysteresis curve between the thermodynamic force such as density/temperature gradients and associated flows.[1,3] Theories[12-15] could predict the sudden L/H transition. The radial electric field (in other words, induced poloidal rotation) plays a main role in theories to cause a bifurcation in the radial flux. Experimental observations[17-19], confirmed changes in poloidal rotation and radial electric field associated with L/H transition. We extend the model theory in Ref.[12-15] to include the time dependence and spatial diffusion. The electric field is used in analysis, but similar argument is possible in terms of rotation. Based on the previous models we employ the model S-curve in phase diagram of the density gradient and the particle flux. We neglect the effect of temperature gradient and consider the case of uniform temperature, since the characteristics of ELMs discussed here is insensitive to the heating power. The periodic occurrence of the burst of the loss

flux from the plasma boundary is predicted by this model. The period of the oscillation, the ratio between the spike width and period, and the region of periodic oscillation in the parameter space are studied. The characteristic nature of the grassy ELMs are confirmed by the model. The radial structure of the transport barrier is investigated, and the important role of the ion viscosity (shear viscosity) is predicted. If the diffusion Plandtl number is large, a thick transport barrier is established, which gives a better enhancement factor for the global energy confinement time. The change of the radial electric field at the L/H transition condition is rapid compared to the plasma parameters. Although rapid it is, there still exist a finite delay time in the response of the electric field and transport coefficient. The effect of this time delay is also analysed. The influence of the temporal variation for the source term is analyzed. If the source term contains a random component, the oscillation period can be chaotic. When the source includes a oscillation component, the frequency of which is close to the natural oscillation period of the plasma loss, the model locking of the oscillation to the external frequency appears. Also the region of the oscillatory solution is expanded. This suggests an experimental method to control an H-mode with favourable ELM oscillations.

The construction of this article is as follows. In § 2, the model of the analysis is discussed. The extension from the previous analyses is shown. In §3, a heuristic argument is given using a zero-dimensional model for the density evolution.

Various characteristic oscillations are found. In §4, the one-dimensional transport equation is solved. Temporal and spatial evolution of the transport barrier is studied. Summary and discussion is given in final sections. Derivation of the model equation is presented in the Appendix A. Transient response associated with the L/H transition is studied briefly in Appendix B.

§2 The Model

We consider the thin layer near the plasma boundary of tokamaks. We take the plasma with one species of ions. The characteristic thickness of this layer is several times of the ion poloidal gyroradius, ρ_p, so that the bipolar particle fluxes, which are driven for instance by the ion loss cone[12,14] and the convective loss of drift wave[12] or the bulk ion viscosity[14], plays an important role in determining the transport coefficient. The bifurcation of the radial electric field structure as well as of the transport coefficient (ratio of the particle flux Γ to the density gradient) has been predicted. Critical condition for the bifurcation is given in either the critical density gradient for given collision frequency[12,13] (as is Fig.1) or in the collision frequency for given gradient[14].

We study the dynamic evolution of the density/electric field profile and transport coefficient in this layer. We take a slab model of this region, and specify the particle flux from the core plasma. This particle flux can be dependent on the transport processes in the edge layer of our interest, because the particle source is influenced by the outflux to the wall. (Such is often the case in actual experiments.) However, in order to investigate the intrinsic properties of the edge plasma, which by itself generates the selfsustaining oscillations, we assume this source flux from core to be an independent constraint. The same argument applies to the plasma in the scrape-off-layer (SoL), and we assume that the boundary condition at the plasma/SoL interface

is also an independent constraint from the dynamic evolution in the layer of our interest. We do not specify the thickness of the layer at this moment, and look for the selfsustaining structure of the oscillation, which does not depend on the choice of the thickness of the layer. This consideration is proved by the results.

According to the previous analyses, we assume that the transport coefficient in this layer has the nature as shown in Fig.1 that the charge neutrality condition[12,13] (or in other words the force balance equation in poloidal direction[14]) shows the bifurcation nature when the gradient parameter

$$\lambda = \rho_p |\nabla n/n|$$

reaches critical values λ_1 and λ_2. The critical values are the functions of relative loss cone loss rate

$$d = \sqrt{a/R} D_e / \nu_i \rho_p^2$$

where a/R is the inverse aspect ratio, D_e is the characteristic diffusion coefficient in the L-phase (which is considered to be anomalous, but we need not specify its characteristics here), n_i is the ion density, and ν_i is the ion collision frequency. When the parameter d is small, the difference between λ_1 and λ_2 becomes large. Critical gradient parameters λ_i and λ_2 come closer if d becomes small[13].

The development of the plasma parameter is described by the

continuity equation

$$\frac{\partial n}{\partial t} = \frac{\partial}{\partial x} D(Z) \frac{\partial n}{\partial x} \qquad (1)$$

which assumes that the particle source in the layer can be neglected. Further assumption is that we neglect the effect of the temperature gradient. The layer of our concern is thin so that the slab model is used in solving the transport equation. In order to describe the temporal and spatial development of the radial electric field and associated transport coefficient, we introduce the equation describing the radial electric field as

$$\varepsilon_{\perp}\varepsilon_0 \, \partial E_r(r,t)/\partial t =$$

$$en_i\rho_p[-\nu_i\sqrt{R/a}\, J_b + \mu_i \nabla^2 (E_r/B_p v_{Ti})], \qquad (2)$$

where $\varepsilon_{\perp}$ is the perpendicular dielectric constant of the magnetized plasma ($\varepsilon_{\perp} = 1+c^2/{v_A}^2$; v_A is the Alfven velocity and c is the speed of light) J_b is the normalized radial current (the amplitude of which is of the order of unity), v_{Ti} is the ion thermal velocity, B_p is the poloidal magnetic field and μ_i is the shear viscosity. The current J_b is not a monotonous function of E_r and causes the bifurcation. The explicit form of J_b depends on the choice of the physics processes causing the bipolar fluxes, and is discussed in the Appendix A. The ion shear viscosity μ_i dictates the spatial structure of the established

radial electric field[20], and hence that of the transport barrier.

We in this article are interested in understanding the qualitative nature of the dynamics, so that we choose a simple analytic form for J_b. As is shown in Refs.[12-15], the explicit forms of J_b and $\lambda_{1,2}[d]$ depends on the modeling of the bipolar fluxes, but the characteristic nature of the transport, that the particle flux can take multiple values as a function of the gradient, are generally derived. We, therefore, discuss the nature of the edge dynamics which is not constrained by the particular choice of the physics modelling of the bipolar fluxes. For that purpose, we choose a simple S-figure curve which is described by the cubic equation as

$$J_b(Z;g) = g-g_0+[\beta Z^3-\alpha Z], \tag{3}$$

as is discussed in the Appendix A. In this symbolic representations, Z is the normalized radial electric field,

$$Z = C\, E_r \rho_p / T_i - Z_0, \tag{4}$$

where the constants C and Z_0 are introduced in order to take this cubic form. [The parameter (α, β) are introduced to simulates the fact that, as in Fig.1, the critical point λ_1 and λ_2 depends on the parameter d (i.e., the relative ratio of the ion loss cone loss). The manifold Z(g) is tightly folded as in the case of small d in Fig.1. The sharpness at the ridge points λ_1 and λ_2

can also be adjusted by parameters (α, β).] The parameter g, which dictates the jump of the diffusion coefficient, is defined as

$$g = \rho_p n' / n\nu_*, \tag{5}$$

and g_0 is a parameter to denote the point of inflection in the curve of $\Gamma(|\nabla n/n|)$. The normalized collision frequency ν_* is the ratio of ν_i to the bounce frequency of ions. The relation between the radial electric field and transport coefficient $D = |\Gamma n/\nabla n|$ is assumed to be a simple form as $D \propto Z$ or

$$D(Z) = (D_{max}+D_{min})/2 + (D_{max}-D_{min})/2 \cdot \tanh Z. \tag{6}$$

In the normalized form Eq.(2) reduces to

$$\varepsilon \frac{\partial Z}{\partial t} = -(D_e/d\rho_p^2) J_b(Z;g) + \mu_i \frac{\partial^2 Z}{\partial x^2} \tag{7}$$

where the coefficient ε is defined as

$$\varepsilon = (1+v_A^2/c^2) B_p^2/B^2 \simeq B_p^2/B^2. \tag{8}$$

The parameter ε indicates a small coefficient showing that eq.(2) has faster time scale than Eq.(1). The parameter regime of our interest is $d \simeq O(1)$. The characteristic time scale in Eq.(1) and the operator $\mu_i \nabla^2$ is of the order of D_e/ρ_p^2 in case

μ_i and D_e have similar magnitude. Solutions Z(g) in L and H phases for the point model[12-15] were given by $J_r(Z;g) = 0$. The curve of D(g), which is determined from the relation $J_r(Z,g)=0$, for the given value of g_0 is shown in Fig.2. The large D and the small D branches correspond to the L and H states, respectively. The transition from L to H or H to L occurs at certain values of g (A→B [L→H] or B'→A' [H→L]). The curve can be defined on each radial point, and the radial and temporal structure Z(x,t) is obtained in the following analysis.

The relation between the parameters (α, β) and plasma parameters depends on the physics modelling on the radial current. If we take the model in Ref.[13], we have an approximate relation as

$$\alpha = 3(1-d)/2(1+d), \quad \beta = \alpha/3 \tag{9}$$

and

$$D_{max} = d, \qquad D_{min} = 0.05. \tag{10}$$

The interpretation is possible using this approximate relation. (See Appendix A.)

§3 Zero-Dimensional Model

In order to have an insight of the ELM physics, we first develop a model of edge plasma dynamics based on the point model (i.e., zero-dimension in space). The model equation which describes the temporal evolution of the edge density is discussed in the appendix A. We in this chapter employ the model equation which is given as

$$dn/dt = S - \tau n \qquad (10)$$

where n is the edge density, S is the source and τ is the rate of the loss. The loss rate τ is the multivalue function of n, and is modeled as

$$\varepsilon [d\tau/dt]/\tau_0^2 = (n/n_0-1) - [\beta(\tau/\tau_0-1)^3 - \alpha(\tau/\tau_0-1)]. \qquad (12)$$

This model assumes that the higher density leads larger loss rate, and the lower density gives smaller loss rate. Since we are treating a simplified one dimensional model, smaller edge density implies that the plasma is less collisional for a given edge gradient. For fixed gradient, the less collisional sate is attributed to the H-mode according to the theoretical models[12-15]. [The edge gradient plays the fundamental role in determining the transport coefficient associated with H/L transitions. The relations with the spatial structure is discussed in the next section.] The parameter ε, which is much

smaller than 1, indicates that the time scale to recover the charge neutrality is much faster than the transport time of density. The normalizing density and loss rate, n_0 and τ_0, correspond to those in the typical values of L-mode. The parameter τ_0^{-1} has the dimension of time. This is the characteristic diffusion time in the layer of our interest in the L-phase, D_e/ρ_p^2.

For the simplicity of the argument, in the following we normalize n, t, S and τ as

$$n/n_0 \to n,\ t\tau_0 \to t,\ S/n_0\tau_0 \to S,\ \text{and}\ \tau/\tau_0 \to \tau. \tag{13}$$

Equation (12) is rewritten as

$$\varepsilon\, d\tau/dt = F(n,\tau) \tag{14-1}$$

with

$$F(n,\tau) = n - 1 - \beta(\tau-1)^3 + \alpha(\tau-1). \tag{14-2}$$

This set of equations is used to study the dynamics associated with L/H transitions and spontaneous oscillation, i.e., ELMs, in the zero-dimensional model. The form of Eq.(12-2) is simplified compared to Eqs.(3) and (6). This simplification does not cause qualitative difference.

§3.1 Oscillation Solution

We first study the nonlinear oscillation in the presence of the static source and in the limit of no time delay, i.e., $\varepsilon \to 0$. The set equations (11) and (14) are solved with the condition S is constant in time.

In the zero ε limit, τ is solved as a function of n through the relation $F(n, \tau) = 0$. Multiple solution is possible for positive values of α as is shown in Fig.3. The parameter α dictates the range of multiple values. If α is a small positive value, then L takes the multiple value in the narrow region of n. If, on the other hand, α becomes large, the range of n for the multiple solution extends wider. At the bifurcation point where $n = n_c$ holds,

$$n_c = 1 \pm (2\alpha/3)(a/3\beta)^{1/3} \qquad (15)$$

the derivative of τ with respect to n diverges, and the jump between branches occurs.

Nonlinear oscillation solution for n is obtained. Figure 4 illustrates a typical example for the evolution of density and loss flux (τn) for the parameter of α=0.5, β=1 and S=1. Pulsative solution for τn is obtained. Figure 5 shows the frequency and ratio of the H-phase duration to the period, η, as a function of source S. Oscillation solution appears in a limited range of the parameters. The value η is discontinuous at the onset parameter for oscillations. The normalized frequency of the oscillation, f, is inversely proportional to α and can be

approximated as

$$f \simeq 3/5\alpha \quad (\text{for } \beta=1 \text{ and } S=1). \tag{16}$$

The boundary for the oscillation solution can be obtained from Eqs.(11) and (14) as

$$S_1 < S < S_2 \tag{17}$$

where

$$S_1 = (1-\sqrt{\alpha/3\beta})[1+(2\alpha/3)\sqrt{\alpha/3\beta}], \tag{18-1}$$

and

$$S_2 = (1+\sqrt{\alpha/3\beta})[1-(2\alpha/3)\sqrt{\alpha/3\beta}]. \tag{18-2}$$

Below this limit S_1, solution converges to the low flux solution, i.e., stationary H-phase. On the contrary, beyond the critical value S_2, the solution merges to the high flux solution, (L-phase). In order to have the oscillation condition, in other words to satisfy $S_1 < S_2$, we have the condition for α as

$$0 < \alpha < 3/4\beta. \tag{19}$$

If α is large and Eq.(19) is not satisfied, then the oscillation solution does not exist. The high-flux branch (L-mode) directly

continues to the low-flux solution (H-mode) at a certain critical value of S.

This result is interpreted as distinction the transition nature by the plasma parameters. As is shown in Fig.1, the difference between λ_1 and λ_2 is small for large d. This case corresponds to the smaller value of α. From the dependence on α, we see that, the selfsustaining oscillation can be possible near the L/H transition boundary for the case of larger value of d. On the contrary, if the parameter d becomes small, (i.e., modelled by larger value of α), the L-region in parameter space is directly connected to the H-region, without passing through the oscillation regime (i.e., Grassy ELM regime). In the following of this section 3, we take β=1 unless specified.

§3.2 Effect of External Noise

The source term can contain noises. In actual situations, the particle flux from the core plasma to the surface is not constant in time but contains noises. The density fluctuations near boundary affects the rate of ionization as well as the magnitude of impinging neutrals from scrape-off layer. These time-fluctuating contribution of the particle source is modelled, and we write

$$S = S_0 + \tilde{S} \tag{20}$$

where S_0 is constant in time and S is assumed to be random. For

the simplicity, we assume that the fluctuation part is Gaussian noise. It is characterized by the average amplitude, $\langle\tilde{S}^2\rangle$ and the standard deviation s.

In numerical calculation, we take the assumption that the time integral of $\tilde{S}$ from t to t+Δt is given by the Gaussian distribution, the average of which is ε_r and the standard deviation of unity (the suffix r denotes 'random').

The resultant oscillation contains random component, so that we evaluate the average frequency $\langle f\rangle$ and the standard deviation σ of oscillations. σ is defined as $\sqrt{\langle(T-\langle T\rangle)^2\rangle}/\langle T\rangle$ where T is the period of the oscillation. Figure 6 illustrates a typical example. The oscillation regime in S-variable extends to lower and higher values of S_0, and $\langle f\rangle$ continuously reduces to zero for $S_0<S_1$ or $S_0>S_2$. The effect is small for the region of $S_1<S_0<S_2$. In the parameter regime where oscillation becomes possible due to the noises, the standard deviation σ is a decreasing function of $\langle f\rangle$. Approximate relation of $\sigma \propto \langle f\rangle^{-0.74}$ is obtained for α=0.5 and $S_0<S_1$. Figure 7 shows a typical example of the oscillations. The period of the oscillation is not constant in time. Intermittency is seen in the appearance of the burst. It is noted, however, the hight of the Burst is less affected and remains almost constant.

§3.3 Influence of External Oscillations

The fluctuation part of S is not necessarily noises, but can contain dominant oscillation component. This is possible, for

instance, when the plasma is rotating and its shape is subject to the helical deformation due to the kink/tearing mode. In this case, the distance between the plasma surface and wall changes oscillatory and, as a result of this, the plasma/wall interaction periodically changes in time, causing the modulation of the particle flux. There is other possibility that this kind of regular temporal change is driven artificially. In order to study the influences of low-mode-number MHD modes on the ELMs or to investigate the method to control ELMs, the study on the effect of external oscillation is important.

We take the model that S is given as

$$S = S_0 + \varepsilon_f \cdot \sin(2\pi\Omega t). \qquad (21)$$

Coefficients S_0, ε_f and Ω are constant in time.

We first study the case that the external oscillation frequency is close to the original frequency (i.e., that in the absence of external oscillation), $\Omega \sim 1$. In this case, we find the mode locking to the externally applied frequency. Figure 8 shows the phase diagram in S_0-ε_f plane. As ε_f increases, the region of oscillation solution extends to wider values of S_0. The oscillation region is divided by three categories. One is the 'almost-unaffected region', where the oscillation frequency is preserved near the original oscillation frequency (the one in the absence of ε_f). This region is localized to the small values of ε_f. The second is the 'locked region', where mode locking (and harmonics as well) takes place. And the third is the

nonperiodic region.

The region, which is denoted as "1" in the figure, denotes the mode locking to the applied frequency. In the periphery of the oscillation regime, the period doubling takes place, i.e., the frequency of the oscillation is one half of the applied one. One third or one quarter harmonics is also found. Figure 8(b) indicates the detailed diagram. Example of time traces are shown in Fig.9. In the case of harmonics, the hesitation is seen. For instance, in the case of the double-period solutions, the hesitation and transition appear one by one. As in the case of the noises, the hight of the burst is not influenced by in comparison with the period. This is because the peak in the loss is determined by the difference of the transport coefficient at the transition point, which is not affected much by the external oscillations.

Other characteristic feature is the solution with nonperiodic burst. In between the '1' and '1/2' regions, there is a regime of non-periodic oscillation. Pulses appears continuously in time, but the distribution of the period have a considerably large standard deviation.

We next study the case where the oscillation frequency Ω is much smaller than the intrinsic frequency. In this case, strong influence takes place near the oscillation boundary, $S_0 \simeq S_1$, S_2. Figure 10 indicate the standard deviation of the oscillation frequency for the case of $\varepsilon_f=0.05$ and $\Omega=1/2\pi$. Intermittent burst of loss is observed as shown in Fig.11.

§3.4 Time Delay in Change of Transport Coefficient

The assumption of $\varepsilon=0$ is idealized. The change of transport coefficient from one branch of solution $F(n,\tau)=0$ to the other one requires a finite time. The finite time delay in the change of transport coefficient reduces the regime of oscillation solution.

We solve Eqs.(11) and (14) for given constant value of S. Figure 12 illustrates the dependence of the frequency on ε. The frequency f reduces as ε increases, and the oscillation finally stops when ε reaches a critical value. Beyond this critical value, the solution of Eqs.(11) and (14) turns out to be a damped oscillation, and the solution converges to the fixed point in the $t\to\infty$ limit. For small but finite value of ε, the boundaries S_1 and S_2 come closer. It is also noticed that the value η, ratio of the period of the H-phase to the oscillation period, shows weak dependence on S.

This critical value can be calculated by studying the stability near the fixed point. If we write n and τ in the vicinity of the fixed point as

$$n = X + u \tag{22-1}$$

$$\tau = Y + v, \tag{22-2}$$

where (X,Y) satisfies

$$XY - S = 0 \tag{23-1}$$

$$F(X,Y) = 0. \tag{23-2}$$

Linearizing Eqs.(11) and (14) in the small u and v limit, we have

$$\begin{bmatrix} du/dt \\ dv/dt \end{bmatrix} = \begin{bmatrix} -X & -Y \\ 1/\varepsilon & (\alpha+3-3Y)/\varepsilon \end{bmatrix} \begin{bmatrix} u \\ v \end{bmatrix} \tag{24}$$

The eigen values Λ of the matrix in the right hand side of Eq.(24) is given as

$$\Lambda = [(\alpha+3-3Y)/\varepsilon]/2 + \sqrt{\{(\alpha+3-3Y)/\varepsilon+Y\}^2 - 4X/\varepsilon} \tag{25}$$

This result gives that the fixed point is stable if

$$\varepsilon > (\alpha+3)/Y-3, \quad X > Y(\alpha+3-3Y) \tag{26}$$

is satisfied. If the fixed point is stable, oscillations decays in time, and converges to the fixed point. Substituting α=0.5 and S=1 (X=Y=1), we have ε>0.5 for the stability near the fixed point, confirming the disappearance of the oscillation solution in Figure 12. Oscillatory solution is obtained for ε<0.5. Figure 13 illustrates the trajectories near the boundary ε=0.5 in the case of α=0.5 and S=1.

§4 Transport Model for ELMs

We develop the one dimensional transport model for the ELM oscillations. The temporal evolution, which was obtained by the heuristic argument in §2 are confirmed. In the one dimensional analysis, we can clarify the spatial structure associated with the periodic transitions between H and L- phases.

§4.1 Model Equations

Model equations consist of the radial transport equation of the density n with the effective diffusivity D, and the diffusion equation of the normalized radial electric field (or poloidal rotation) Z with the viscous diffusivity μ. The effective diffusivity D, which is a function of Z, can have multiple values. The basis of this model equation is discussed in the appendix. Diffusion Equations contain a nonlinear force with respect to the density gradient and are given as

$$\frac{\partial n}{\partial t} = \frac{\partial}{\partial x} D(Z) \frac{\partial n}{\partial x} , \tag{27}$$

$$\varepsilon \frac{\partial Z}{\partial t} = -N(Z;g) + \mu \frac{\partial^2 Z}{\partial x^2} , \tag{28}$$

$$N(Z,g) = g - g_0 + [\beta Z^3 - \alpha Z], \tag{29}$$

and

$$D(Z) = (D_{max}+D_{min})/2 + (D_{max}-D_{min})/2 \cdot \tanh Z. \qquad (30)$$

In writing explicit forms of N and D, we normalize as

$$x/\rho_p \to x,\ D/D_0 \to D,\ d\mu_i/D_0 \to \mu,\ tD_0/\rho_p^2 \to t,\ \text{and}\ \Gamma\rho_p/D_0 n_0 \to \Gamma.$$

The normalizing density n_0 is chosen so as to satisfy $g_0=1$ and $g = 3n^{-2}(dn/dx)$. We use the relation

$$\varepsilon = d(\rho/\rho_p)^2 \qquad (31)$$

noting $v_A<<c$. The normalizing parameter D_0 is the typical value of the diffusion coefficient in the L-phase. The coefficient μ is the diffusion Prandtl number P_D dictating the profile[21]. Parameters g_0, α, β, D_{max}, D_{min} and μ are treated as constant.

Equation (28) is a kind of time dependent Ginzburg-Landau equation or the one which is used to analyse the reaction diffusion system in chemical reactions. The system contains so-called slow manifold structure due to the assumption with respect to the time scales.

§4.2 Periodic formation of the Transport Barrier (ε=0 case)

We first take the condition that $\varepsilon=0$ (i.e., $\partial Z/\partial t = 0$) to solve the temporal evolution of the density.

The region of our interest is a slab near the plasma edge, $-L<x<0$. As the boundary condition at the plasma edge ($x=0$), we impose the constraint that

$$(n'/n)^a n^b = \text{const.} \quad (\text{at } x=0) \tag{32}$$

is used. In the following we mainly discuss the case of $a=1$ and $b=0$. This simplified form is approximately reproduce the two-dimensional analysis in the scrape-off layer plasma[22]. For the boundary condition at the core side ($x=-L$), we give the particle flux as

$$\Gamma = \Gamma_{in}. \quad (\text{at } x=-L) \tag{33}$$

Solving Eqs.(28) and (29) we find the state with the periodic oscillations of the edge density n_s and the loss flux Γ_{out} in the restricted parameter space between the L and H phases. (Γ_{out} is defined as the particle flux at $x=0$.) In Fig.14 (a), (b) and (c), we show the temporal evolution of the edge density and Γ_{out}, which corresponds to the origin of the H_α burst in experiments. The parameters are; $g_0=1$, $\alpha=0.2$, $\beta=0.2$, $D_{max}=3$, $D_{min}=0.01$, $\mu=1$,

$$r_n = -n/n' \quad (\text{at the edge}) \tag{34}$$

is chosen as 1.25, and $\Gamma_{in} = 3$.

The existence of intermediate state of L and H phases is seen in the radial structure of the density and the effective

diffusion coefficient. In Fig.14 (d) and (e), their radial structures are shown at the time of good confinement and the poor confinement. The temporal-spatial developments of the density and diffusion coefficient are shown by the bird's eye view in Fig.14 (f) and (g).

These oscillating solutions are possible in the intermediate state between L and H phases, and are attributed to ELMy-H mode. The time averaged density is somewhat between the one in L phase and the H's. Figure 15 illustrates the frequency and the average ratio of H-phase period (η-value) as a function of Γ_{in}. The result is similar to those in a simple zero-dimensional analysis. Figure 16 shows the phase diagram in Γ_{in}-r_n plane. Three regions are identified; H-region, L-region and ELM region.

The parameter region in which the ELMy-H mode appear is found to be

$$D_m/g_m < \Gamma_{in} r_n^2 < D_M/g_M, \tag{35}$$

where

$$g_m = g_0 - 2\beta(\alpha/3\beta)^{3/2}, \tag{36-1}$$

$$g_M = g_0 + 2\beta(\alpha/3\beta)^{3/2}, \tag{36-2}$$

$$D_m = D(Z=\sqrt{\alpha/3\beta}), \tag{36-3}$$

and

$$D_M = D(Z = -\sqrt{\alpha/3\beta}). \tag{36-4}$$

In this parameter regime, the cross point of the curve of hysteresis and the g value at the edge becomes unstable and the solution of the limit cycle on g and D space (see Fig. 2) appears. When Γ_{in} becomes large so as to satisfy

$$\Gamma_{in} r_n^2 > D_M/g_M, \tag{37}$$

we find the stationary L state; and the H state with large density gradient is found in the parameter region

$$\Gamma_{in} r_n^2 < D_m/g_m. \tag{38}$$

Therefore the ELMy-H state found here is the mesophase of L and H phases. If the condition

$$D_m/g_m > D_M/g_M \tag{39}$$

holds, no oscillation is allowed. In such a case, direct transition form L to H phase (or vice versa) when Γ_{in} changes.

This result confirms those in the zero-dimensional modelling. As is shown in Fig. 1, the difference between λ_1 and λ_2 is small for large d. The selfsustaining oscillation can be possible near the L/H transition boundary for the case of larger value of d. In addition to it, the transport analysis yields the

new constraints on the gradient near edge. The sharpness of the edge gradient at the plasma/SoL interface affects the appearance of the ELMs. On the contrary, if the parameter d becomes small, (i.e., modelled by larger value of α), the L-region in parameter space is directly connected to the H-region, and even the overlapping of them occurs. The transition between H and L phase takes place without passing the oscillation regime (i.e., Grassy ELM regime).

§4.3 Structure of Transport Barrier

Transport barrier is formed in a phase of density rise. Smooth change of D is formed due to the viscosity μ[20]. The thickness of the barrier, Δ, is estimated as

$$\Delta \simeq \sqrt{2\beta\mu/\alpha} \tag{40}$$

in the small μ limit. Numerical calculation gives $\Delta \propto \mu^{0.44}$, as shown in Fig.17, confirming this analysis. (This numerical result is obtained in the situations where L satisfies $L \gg \Delta$, so that Δ is not limited by the computation region.) In this region, $-\Delta < x < 0$, there exists the poloidal rotation. The radial width Δ is different from the width of the density inversion region.

We study the parameter dependence of the period τ of the oscillation. Results are illustrated in Fig.17(b) and 18. The numerical computation gives

$$\tau \simeq C\alpha r_n \Delta D_M^{-1}, \tag{41}$$

where C is a numerical coefficient of the order of unity. As is shown in Eq.(32), r_n is bounded in a narrow region to realize the oscillation. If the ratio r_n^2/D_M and other parameters are fixed, we have

$$\tau \propto D_M^{-0.5} \tag{42-1}$$

in a wide range of parameters. On the other hand, if the ratio $\Gamma_{in} r_n^2$ and other parameters are fixed, we have

$$\tau \propto \Gamma_{in}^{-0.5}. \tag{42-2}$$

Figure 18 shows that the oscillation is generated by the periodic establishment and decay of the transport barrier, the thickness of which is determined by the viscosity. If the layer of the analysis L is much longer than Δ, L does not effect the oscillation frequency. The transport in the layer of L does not give the characteristic time scale. This provide the basis, *a posteriori*, that the specific assumption for the core plasma is not necessary in developing the modelling of ELMs of our interest.

The ratio of the time interval of good confinement τ_H to τ, $\eta=\tau_H/\tau$, represents how the mesostate is close to the H-mode. (In the H-mode, $\eta=1$, and $\eta=0$ for the L-mode). In the region of Eq.(32), η takes intermediate values between one and zero. η is

a decreasing function of $\Gamma_{in}r_n^2$, and is discontinuous at the boundaries D_m/g_m and D_M/g_M. For oscillating solutions, η takes largest value

$$\eta = \eta_{max} \text{ at } \Gamma_{in}r_n^2 = D_m/g_m. \tag{43}$$

η_{max} increases and approaches to unity if D_m becomes closer to D_{min}. This is confirmed by reducing α as keeping the ratio α^3/β constant (i.e., reducing D_m to D_{min} by fixing g_m). For instance, by taking $\alpha=0.2$ and $\beta=\alpha^3$, η can be greater than 0.95, i.e., the period is 20 times longer than the pulse width. (See Fig.19.)

§4.4 Effect of Time Delay in the Response of D

The finite time delay in the response of diffusivity in jumping at the critical value of g gives rise to the damped oscillation and reduces the range of the stationary oscillation regime.

Example is shown in Fig.20 with various values of ε and other parameters are unchanged. As ε increases, the change of the flux becomes diffused. This is the same as in the simple argument of the zero-dimensional model.

In obtaining the spatial structure of n and D, we see that the qualitative character, such as the thickness of the transport barrier, does not change compared to the case of the zero ε limit.

For the parameter of our interest, ε is of the order of

$(\rho/\rho_p)^2$, i.e. order 1/100. Therefore, the analysis with $\varepsilon=0$ provides a sufficiently good approximate solutions.

§5 Summary and Discussion

In summary, the theoretical model of ELMs are developed by extending the bifurcation model for H/L transition to the time-dependent diffusive media near tokamak surface. Time-dependent Ginzburg-Landau model equation with spatial diffusion is applied. A periodic solution of the plasma density and outflux is found recovering the sequence of the burst of plasma loss.

The transition has the nature that the transport coefficient changes very rapidly at the critical condition for plasma parameters. This nature leads a sharp rise of the loss flux in each period of oscillations. The loss rate then reduces slowly, with the time scale of L-mode transport, according to the gradual change of the edge plasma parameters. As the plasma parameter changes far enough to encounter the transition condition to the good confinement states. This model reproduces the oscillations in which the decay time of the loss and period are comparable. The region in which this nonlinear oscillation occurs is identified in the parameter space; oscillations appear near the H/L mode boundary. These features are consistent with experimental observations of the Grassy ELMs. In addition to them, this model also predicts that, at the end of the each burst, the sudden reduction of loss occurs. This awaits an experimental confirmation, which would be possible by careful study on the energy deposition onto the divertor plate with high time resolution. (The observation on the H_α/D_α line would not be suitable for this examination, because this intensity may be

prolonged by the recycling .)

The mesophase is found near the plasma boundary. The width of the transport barrier was found to be proportional to $\sqrt{P_D}$. The frequency of the sequential burst of losses is characterized by the time ρ_p^2/D_0 and the numerical coefficient characterizing the nonlinear potential. Also the parameter dependences of the period and "H-ness" η are studied.

This study shows the important role of the diffusion Prandtl number in determining the temporal/spatial structure of the transport barrier. When the thickness of the transport barrier is larger, the better enhancement in the global energy confinement time is expected[23]. The viscosity near the plasma edge requires future analysis in order to provide more dependable picture of the ELMs.

The occurrence of the periodic transitions between H and L states are anticipated in the presence of impurities[10]. It is shown that the periodic oscillation is possible even in the absence of impurities. The inclusion of impurities would gives rise a further variety in the oscillation phenomena in ELMs. This requires a further research. The analysis in this article is developed using a simplified analytic form of the transport coefficient. If one employs more exact form of D[g] as is presented in Appendix, absolute values may change (e.g. for the frequency, η-value and so on.) However, the qualitative nature of the nonlinear oscillation and parameter dependences such as on the viscosity or times scales does not alter.

The present analysis on the appearance of the self sustained

oscillation clarifies the expected parameter region for the continuous small ELMs. The importance of the parameter $d \propto D_e/\nu_i \rho_p^2$ is found. If we employ the model in Ref.[13] for the radial current, then the condition for the oscillation, $D_M/g_M > D_m/g_m$, is rewritten as (using the relation between α, β and d),

$$d > 0.22.$$

We have

$$\begin{cases} 0.2 < d < 1 & \text{(Grassy ELMs)} \\ 0 < d < 0.2 & \text{(hard L/H transition).} \end{cases}$$

If this parameter d is large, then the difference between λ_1 and λ_2 is small. In such a situation, the selfsustaining oscillation can be possible near the L/H transition boundary. In addition to it, the transport analysis yields the new constraints on the gradient near edge. The sharpness of the edge gradient at the plasma/SoL interface affects the appearance of the ELMs. Noticing the parameter dependence of d, we see that d increases if the edge diffusivity D_e increases and other parameters are not changed. This would be one of the origin of the expansion of the Grassy ELM regime under the Ergodic Magnetic Limiter. The proper range of enhancement of the electron loss in the L-phase is helpful in achieving the ELMs in wider plasma parameters. On the contrary, if the parameter d becomes small, (i.e., modelled

by larger value of α), the L-region in parameter space is directly connected to the H-region, and even the overlapping of them occurs. The transition between H and L phase takes place without passing the oscillation regime (i.e., Grassy ELM regime). The transition to the H-mode in this occasion is often triggered by heat pulses. We simulate the transient phenomena in Appendix B.

The roles of fluctuations in the source flux or external oscillations are also studied. It is found that they cause the chaotic oscillations of n and Γ_{out}. They also extend the region of ELMs to the wider segment in the parameter space. It is also noted that the hight of the burst in loss is not affected much by the introduction of the temporal variation of the sources. The period is much more influenced. This nature can be compared to the experimental observations. In the case that the external oscillation amplitude is large enough, the oscillations, the frequency of which is locked to the external one, appears in the wide parameter range. This would provide an experimental method to control the ELMs with favourable frequency (such as grassy ELMs) under more general situations, not necessarily in the vicinity of the L/H boundaries. The urgency to control ELMs is now widely recognized. One candidate for the state with good confinement, which is free from impurity accumulation and does not yield a serious condition on the wall erosion, is an H-mode with grassy ELMs. More theoretical and experimental research would be requested to realize a dependable controlling method.

Acknowledgements

Authors acknowledge discussions with Prof. T. Ohkawa, Dr. Y. Miura and JFT-2M Group, Dr. S. Konoshima and DIII-D group. Comments by Prof. A. Lichtenberg is also appreciated. This work is partly supported by the Grant-in-Aid for Scientific Research of MoE Japan, and by the collaboration program between universities and JAERI on fusion research.

Appendix A: Model Equation

In this appendix, we discuss the model forms of the transport equation associated with the L/H transitions. The present models on the L/H transition take into account the bifurcation of the radial electric field (and associated poloidal rotation). The radial current near plasma boundary can be written as

$$J_r = J_b = J_{orbit} + J_{conv} + J_{bv} + J_{cx} \qquad (A1)$$

where terms in the right hand side correspond to the currents driven by the ion orbit loss, convective loss of drift waves, the bulk ion viscosity, and the charge exchange loss, respectively. (The suffix b indicates that the process is strong near plasma boundary.) In order to study the radial profile of the radial electric field, the shear viscosity is also important, and we write

$$J_r = J_b + J_v \qquad (A2)$$

where J_v is the radial current driven by the shear viscosity. The temporal equation dictating the radial electric field is given as

$$\varepsilon_\perp \varepsilon_0 \, dE_r/dt = - J_r \qquad (A3)$$

Using the E_r and E_r' dependences of J_b, the theoretical modelling has been developed. First brief review is made. The relation $J_b = 0$ was used as the basic equation to obtain the multiple states associated with the L and H modes in a stationary state. It has been found that the equation $J_b=0$ gives multiple solutions, which allows the bifurcation, and that transport coefficient is the decreasing function of the electric field inhomogeneity. When the radial electric field piles up near the boundary, the anomalous diffusion and the loss cone loss as well as the bulk viscosity are reduced. The particle flux Γ_r and the transport coefficient D, which is defined by $-\Gamma/\nabla n$ is calculated as a function of the gradient near the plasma boundary. Figure A1 illustrates Γ and D as a function of $\lambda=-\rho_p\nabla n$. The solution of the radial electric field is also obtained for the three branches of the function $\Gamma(\lambda)$, i.e., L-branch (large flux) H-branch (small flux) and intermediate (unstable) branch. The coefficient D is an increasing function of the radial electric field. The dependence of the critical gradient λ_c on the plasma parameter has been studied. A rough estimate of the criterion is given as

$$d\cdot\lambda_{c1} \sim 1 \qquad (A4)$$

for usual parameters. ($d=\sqrt{a/R}D_e/\nu_i\rho_p^2$.)

In order to have a physics insight of the dynamic problem, which is the subject of this article, we here use a simplified functional dependence for the curve of $D(\lambda)$. The model form for

$D(\lambda)$ is given by the implicit function

$$D(Z) = (D_{max}+D_{min})/2 + (D_{max}-D_{min})/2 \cdot \tanh Z \qquad (A5)$$

and Z is a solution of the nonlinear equation $N(Z;g)=0$ with

$$N(Z,g) = g-g_0+[\beta Z^3-\alpha Z]. \qquad (A6)$$

and

$$g = d\lambda. \qquad (A7)$$

In this symbolic representations, Z is the normalized radial electric field,

$$Z = C\ E_r \rho_p / T_i - Z_0 \qquad (A8)$$

where the constants C and Z_0 are introduced in order to take the form Eq.(A5). (C and Z_0 are of the order of unity.) The real form $D(\lambda)$ is not exactly expressed by the cubic polynomial, but this simplification can keep the qualitative nature of the response function of $\Gamma(\lambda)$ and would be more suitable to study the physics of the dynamic processes.

The nonlinear Equation $N(Z;g)=0$ is derived from the relation $J_b = 0$ in the stationary limit. As was discussed, J_{orbit}, J_{conv} and J_{bv} have nonlinear dependence on E_r, giving rise to the nature of the bifurcations in $\Gamma(\lambda)$. For instance, J_{orbit} is

approximately given as

$$J_{orbit} = [C_F n_i \nu_i \rho_p / \sqrt{a/R}] \exp\{-Z^2\}. \tag{A9}$$

(C_F is a constant of the order of unity.) From this consideration, we model

$$J_b = J_1 \hat{J}_b(Z;g), \tag{A10}$$

$$\hat{J}_b = N(Z;g) \tag{A11}$$

and the normalizing coefficient J_1, which has the dimension of the current is given as

$$J_1 = C_F n_i \nu_i \rho_p / \sqrt{a/R} \simeq n\nu_* \ (T/erB) \tag{A12}$$

except a numerical coefficient of the order of unity. The shear viscosity current is written as

$$J_v = \nabla [e\rho_p n_i / v_{Ti}] \mu_i \nabla (E_r/B_p), \tag{A13}$$

where μ_i is the ion viscosity. Form these modellings on the shape of the current, we rewrite Eq.(A3) as

$$\varepsilon \frac{\partial Z}{\partial t} = -(D_e/d\rho_p{}^2) J_b(Z;g) + \mu_i \frac{\partial^2 Z}{\partial x^2} \tag{A14}$$

where the coefficient ε is given as

$$\varepsilon = (1+v_A^2/c^2)B_p^2/B^2 \simeq B_p^2/B^2. \tag{A15}$$

The density develops according to the continuity equation as

$$dn/dt = \nabla D[Z;g]\nabla n \tag{A16}$$

For usual plasma parameters, we have ε is of the order of 1/100.

The relation between the plasma parameters and model coefficients (α, β, D_{max}, D_{min}) can be made if the physics model on the radial current is chosen. As an example, we study the case in the model of Ref.[13]. In this model, relations

$$\lambda_1 \propto 1/d, \tag{A17-1}$$

and

$$\lambda_2 \simeq \text{const} \tag{A17-2}$$

holds as a rough estimate. At the transition point, λ_1 and λ_2, the flux Γ is a weak function of d. We therefore have the estimations

$$g_M = 2/(1+d), \tag{A18-1}$$

$$g_m = d/(1+d) \tag{A18-2}$$

and

$$D_{max} = d, \tag{A19-1}$$

$$D_{min} = 0.05. \tag{A19-2}$$

There is a free parameter in the relation between (α, β) and d. One candidate is

$$\alpha = 3(1-d)/2(1+d) \tag{A20-1}$$

and

$$\beta = (1-d)/2(1+d). \tag{A20-2}$$

If one uses the other model for J_r, parameters (α, β, D_{max}, and D_{min}) have other dependence on plasma parameters.

Much simplified analysis is performed by making the zero dimensional model. If one integrates Eq.(A16) within a thin layer near the edge, $-L<x<0$ (x is the distance from the edge), we have

$$d\bar{n}/dt = \Gamma_{in}/L + D\overline{\nabla n}/L \tag{A21}$$

where the over bar denotes the spatial average, and Γ_{in} is the flux at the location x=-L. The loss time τ and the source term S

are introduced as

$$\tau\bar{n} = -D\overline{\nabla n}/L, \tag{A22-1}$$

$$S = \Gamma_{in}/L. \tag{A22-2}$$

By this notations, we have a model equations for the zero-dimensional analysis as

$$d\bar{n}/dt = S - \tau\bar{n} \tag{A23}$$

where τ has the same characteristics of the multiple states as the transport coefficient D.

Appendix B: Transient Process st the L/H-Transition

This formulation of the transport property near the plasma edge can be applied to the transient processes at the L/H transition. The zero-dimensional model is used to show an example of the transition triggered by the short pulse. In experiments, at the plasma parameters which is close to the L/H transition boundary, the transition is often observed to be triggered by a short pulse such as the heat pulse by the sawtooth crash. When the plasma parameter is not close enough to the boundary, such pulses can cause the short H-mode. These phenomena are simulated.

Zero-dimensional model is solved for the parameter of α=1.5. In this case, the difference between n_{c1} and n_{c2} is large, so that the region of H-phase directly connects to the region of L-phase as a parameter of S. We choose two neighbouring values of S: 0.5 and 0.51. For the case of S=0.5, two stable states (one is with large τ and the other is with small τ) exists. We take a simple example of favourable pulse that

$$S = \begin{cases} S_0 & t<10 \text{ or } t>10.5 \\ S_0/2 & 10<t<10.5 \ . \end{cases} \qquad \text{(B1)}$$

Figure B_1 illustrates the results of S_0=0.75 (a) and 0.765 (b). (Parameter ε is taken to be 1/20, α=1.5, β=2.0.) In the case of Fig.B1(a), the short pulse kick the plasma into the state of H,

and the plasma remains in the H-state after the pulse goes away and the flux comes back to the original value. On the contrary, if the parameter is a little bit away from the transition point, in the case of S_0=0.765, the pulse gives rise to the short period of H-states, but the states collapse and back to the L-state after the pulse passes away. The short H-phase, which ends with one burst of loss, is caused by the short pulsative change in the flux from the core plasma. The duration time of the short H-phase is much longer than the pulse width. It is determined by the cycle time of the trajectory in Fig.B1(b).

This result explains the effect of heat pulses near the L/H transition. As the parameter approaches to the transition point, according to the ASDEX or JFT-2M reports, short H-phases appear associated with the heat pulses, and finally the heat pulse causes the transition to the stationary H-phase.

References

[1] M. Keilhacker, G. Becker, K. Bernhardi, et al.: Plasma Phys. Controlled Fusion **26** (1984) 49.

[2] F. Wagner, G. Becker, K. Behringer, et al.: Phys. Rev. Lett.: **49** (1982) 1408.

[3] The ASDEX Team: Nucl. Fusion **29** '1989) 1959.

[4] P. Gohil, M. A. Mardavi, L. Lao, et al.: Phys. Rev. Lett. **61** (1988) 1603; D. H. Hill, T. Petrie, M. A. Mardavi, et al.: Nucl. Fusion **28** (1988) 902; D. P. Schissel, K. H. Burrel, J. C. DeBoo, et al: Nucl. Fusion **29** (1989) 185.

[5] DIII-D Team, in Plasma Physics and Controlled Nuclear Fusion Research, 1990, Proc. 13th International Conf., Washington DC USA, (1990) Paper CN-53/A-1-4.

[6] T. Shoji, and JFT-2M Group, in Controlled Fusion and Plasma Physics (Proc. 17th European Conf., Amsterdam, 1990), Part3, (1990) 1452.

[7] Y. Miura and JFT-2M Group, in Plasma Physics and Controlled Nuclear Fusion Research, 1990, Proc. 13th International Conf., Washington DC USA, (1990) Paper CN-53/A-4-6.

[8] T. Osborne, K. H. Burrell, T. Carlstrom, et al: Bull. Am. Phys. Soc. **35** (1990) 1975.

[9] Y. Miura and JFT-2M Group, private communications (invited paper presented in the 3rd H-Mode Workshop (JET, 1991)

[10] T. Ohkawa, S.-I. Itoh, and K. Itoh, Kakuyugo Kenkyu, **59** (1988) 488.

[11] F. Wagner, F. Ryter, A. R. Field, et al.: in Plasma Physics

and Controlled Nuclear Fusion Research, 1990, Proc. 13th International Conf., Washington DC USA, (1990) Paper CN-53/A-4-2.

[12] S.-I. Itoh, K. Itoh, Phys. Rev.Lett. 60 (1988) 2276.

[13] S.-I. Itoh and K. Itoh, Nucl. Fusion 29 (1989) 1031.

[14] K. C. Shaing, E. C. Crume, Phys. Rev. Lett. 63 (1989) 2369.

[15] S.-I. Itoh and K. Itoh; J. Phys. Soc. Jpn. 59 (1990) 3815.

[16] S.-I. Itoh, K. Itoh, A. Fukuyama, Y. Miura and JFT-2M Group: Research Report NIFS-87 (National Inst. Fusion Science, 1991) submitted to Phys. Rev. Lett. for publication.

[17] R. J. Taylor, M. L. Brown, B. D. Fried, H. Grote, J. R. Liberati, G. J. Morales, P. Pribyl, D. Darrow, M. Ono, Phys. Rev. Lett. 63 (1989) 2365.

[18] R. J. Groebner, K. H. Burrel, R. P. Seraydarian, Phys. Rev. Lett. 64 (1990) 3015.

[19] K. Ida, S. Hidekuma, Y. Miura, T. Fujita, M. Mori, K. Hoshino, N. Suzuki, T. Yamauchi, JFT-2M Group,, Phys. Rev. Lett. 65 (1990) 1364.

[20] E. Yahagi, K. Itoh, M. Wakatani, Plasma Physics and Controlled Fusion30 (1988) 995.

[21] S.-I. Itoh: J. Phys. Soc. Jpn. 59 (1990) 3431.

[22] S.-I. Itoh, N. Ueda, and K. Itoh: Plasma Phys. Controlled Fusion 32 (1990) 415.

[23] K. Itoh, and S.-I. Itoh, Comments on Plasma Phys. Controlled Fusion 14 (1991) 1.

Figure Captions

Fig.1 Normalized particle flux Γ as a function of the gradient parameter λ for various values of d. The momentum loss by neutral particles is not taken into account. (Quoted from Ref.[13] with corrections).

Fig.2 Model of effective diffusivity D (i.e., ratio of the particle flux to the density gradient) as a function of gradient parameter g. See text for the definition and normalization. (α=1, β=1, D_{max}=3, D_{min}=0.1, g_0=1).

Fig.3 Model of the loss rate as a function of density in the zero-dimensional model (solid line; α=0.5, β=1.0). Dotted line indicates the line of constant loss (example of τn=1). At critical values of S, transitions occurs.

Fig.4 Example of the time trace of the density (a) and loss (b) (zero-dimensional model). Parameters are S=1.0 and α=0.5 (β=1, ε=0). Normalized values are plotted. Periodic oscillations are recovered, which are characterized by the sharp burst of the loss. (c) shows the trajectory (n, τn).

Fig.5 Oscillation frequency f as a function of S, (a), and

the rate of H-phase to the period η, (b) are shown. Parameters are α=0.5 β=1, and ε=0. Discontinuous change appears at S_1 ($\sim$ 0.67) and S_2 ($\sim$ 1.21).

Fig.6 Average oscillation frequency $\langle f \rangle$ and standard deviation σ in the presence of noises. Noise amplitude is chosen as ε_n=0.05. Other parameters are α=0.5 β=1 and ε=0. Frequency in the absence of the noise is also plotted (dotted-dashed line), showing that the effect is small for the parameter $S_1 < S < S_2$.

Fig.7 Typical example of the time trace in the presence of the noise. (S_0=0.61, ε_n=0.05, α=0.5, β=1).

Fig.8 Phase diagram in the presence of the external oscillation in the source is plotted on the plane of DC component S_0 and oscillation amplitude ε_f. Frequency of the external oscillation is fixed to be Ω=1, and (α=0.5, β=1). Mode locking is found in the wide parameter regime. Locking to the subharmonics is also found. Numbers j/k (such as 1, 1/2, 1/3, 2/3, 3/4 ...) indicates that the mode locking with j/k harmonics to the external frequency occurs in this region. Expanded diagram is given in (b). Original oscillation prevails in the dotted region. In shaded area, random oscillation takes place.

Fig.9 Typical time traces for the mode-locked oscillations. Mode locking to the fundamental oscillation (a) and to subharmonics (b: 2/3 period, c: 1/2 period and d: 1/3 period). Parameters are ε_f=0.25, Ω=1, α=0.5, β=1, and S_0=0.65 (a), 0.61 (b), 0.55 (c) and 0.505 (d).

Fig.10 Effect of the low frequency external oscillation. Standard deviation of the oscillation period is plotted for the parameters of ε_f=0.05, Ω=1/2π and (α=0.5, β=1).

Fig.11 Example of the time trace in the presence of low frequency external oscillations. ε_f=0.05, Ω=1/2π, α=0.5 and β=1. Intermittency of the bursts is observed. S_0 is 0.71 (a), 0.69 (b), 0.66 (c), 0.64 (d), and 0.625 (e), respectively.

Fig.12 Oscillation frequency as a function of time delay ε. Parameters are S=1, α=0.5, and β=1. Persistent oscillation is not possible for ε>0.5.

Fig.13 Trajectories near the stability boundary for S=1 and (α=0.5, β=1). The stability criteria for the fixed point is ε=0.5. (a), (b) and (c) shows cases of ε=0.4, 0.5 and 0.6, respectively. In (a), limit cycle is seen. In (c), orbits converge to the fixed point. (b) corresponds to the marginal stability.

Fig.14 Temporal evolution of the edge density n_s (a) and outflux Γ_{out} (b). Parameters are μ=1, Γ_{in}=3, r_n=1.25, α= β= 0.2, D_{max}=3, and D_{min}=0.01. Trajectory in (n_s-Γ_{out}) space is given in (c). Spatial profiles of density (d) and diffusivity (e). Time slice is denoted by arrows in (a). Solid and dashed lines show before the burst and end of the burst, respectively. Bird's eye view for the developments of the density and diffusivity are shown in (e) and (f).

Fig.15 Dependence of the frequency and 'H-ness' parameter η, as a function of the source fluxes. r_n=1.25, Γ_{in}=3 and other parameters are standard as in Fig.2.

Fig.16 Region of the oscillation solution. Parameter space (D_{max}-r_n^2 in(a) and D_{min}-r_n in (b)) is divided into H-phase, L-phase and Elmy phase. ELMy region appears between those for H-phase and L-phase. At large α-values, the H-regime directly connects to the L-regime. Parameters are as in Fig.2.

Fig.17 The μ-dependences of the thickness of the transport barrier (a) and the oscillation period (b). α=β=0.2, and other parameters are standard values as in Fig.14. Dependence as $\Delta \propto \mu^{0.43}$ and $\tau \propto \mu^{0.44}$ is found, confirming the analytic estimates.

Fig.18 Oscillation period as a function of the layer width L. When the length L of the calculation is much longer than the width of the transport barrier Δ, the oscillation frequency is not influenced by L. (Other parameters are standard as in Fig.14.)

Fig.19 Example of sharp loss pulses, for which the pulse width is less than 1/10 of the oscillation period. Parameters are $\alpha=0.2$, $\beta=\alpha^3$, $r_n=0.45$ near the boundary between H and ELMy states. (Other parameter si same as in Fig.14.)

Fig.20 Temporal evolution of the loss flux in case the delay time is long ($\varepsilon>0$). Case of $\varepsilon=0.1$ (a) is compared to the case of $\varepsilon=0$ (b) and 0.5 (c). If ε is finite, the oscillation frequency becomes small, and the pulse of the loss is less sharp. In the case of (c), the final solution converges to the L-state.

Fig.A1 Relation between the flux, transport coefficient and radial electric field as a function of the normalized gradient at edge. (See. Ref.[15].)

Fig.B1 Temporal change of edge density and flux associated with the short pulsative reduction of source flux in the period of $10<t<10.5$. Parameters are $\alpha=1.5$, $\beta=2.0$,

ε=1/20 and S_0=0.75 (a) and 0.765 (b). $S=S_0/2$ in that short period, and is S_0 elsewhere. The transition to the H-mode is triggered in (a), but the state returns back to the L-mode in (b). The duration of the short H-phase in (b) is much longer than the pulse width.

Fig. 1

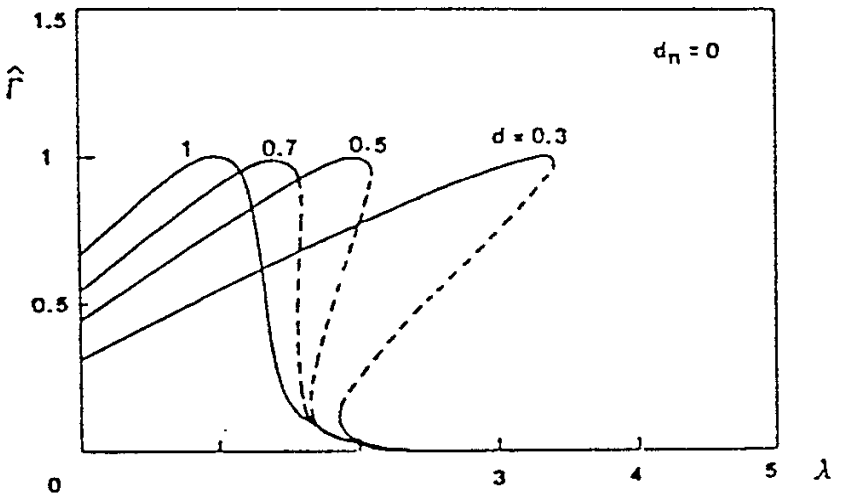

Fig. 2

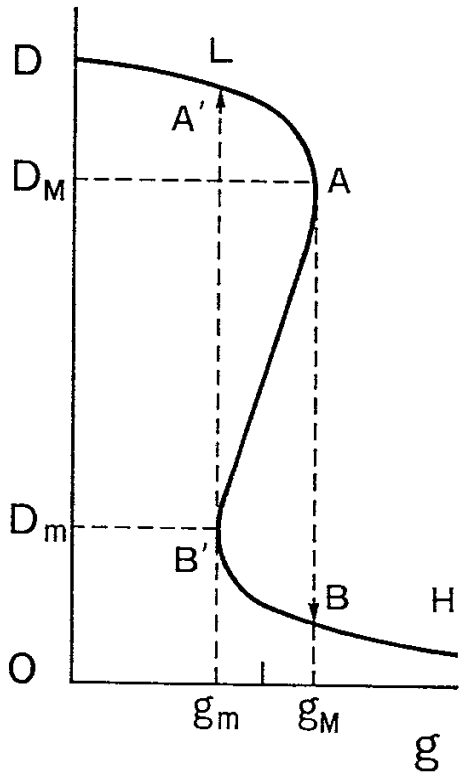

Fig. 3

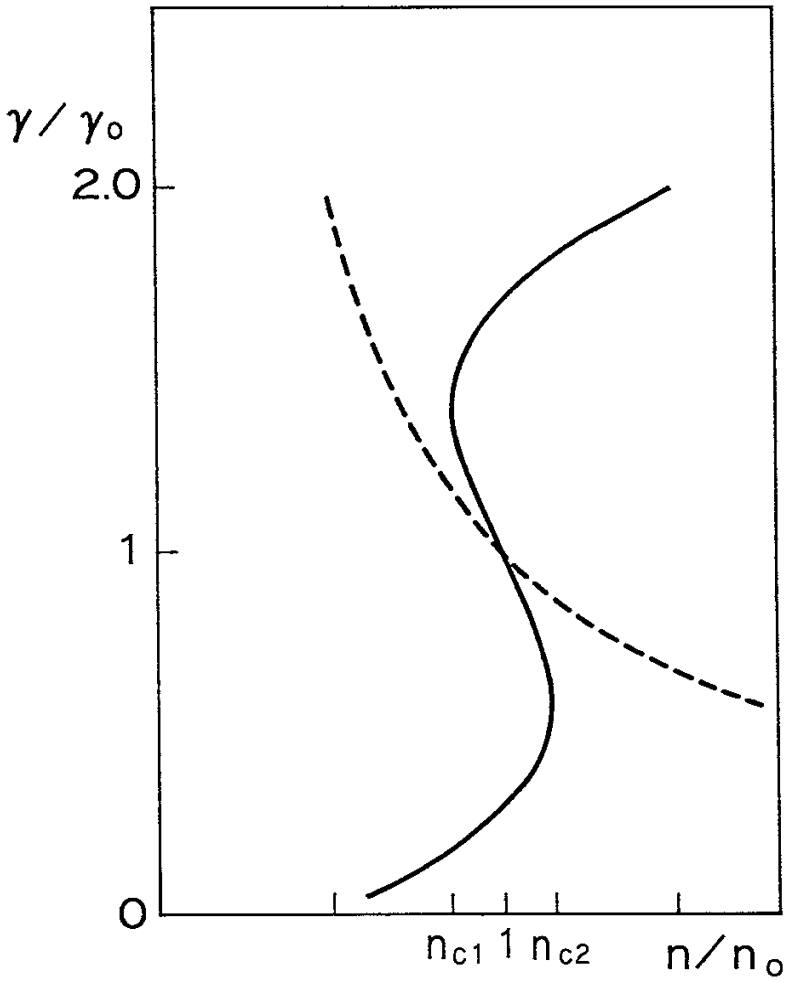

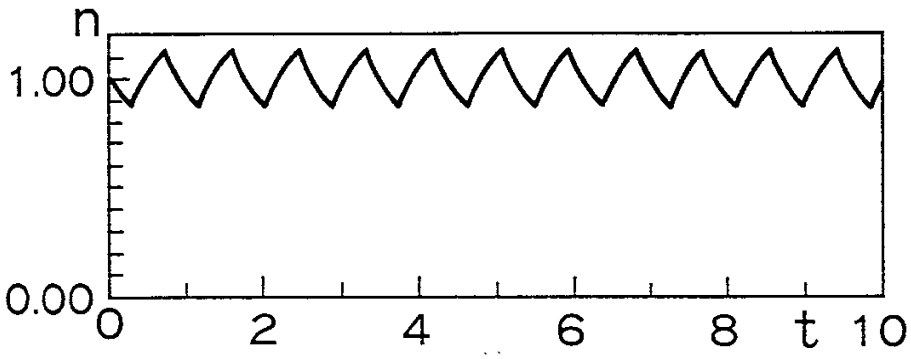

Fig. 4(a)

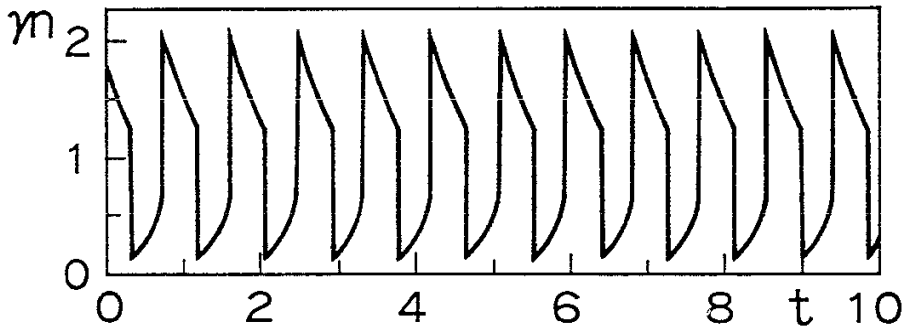

Fig. 4(b)

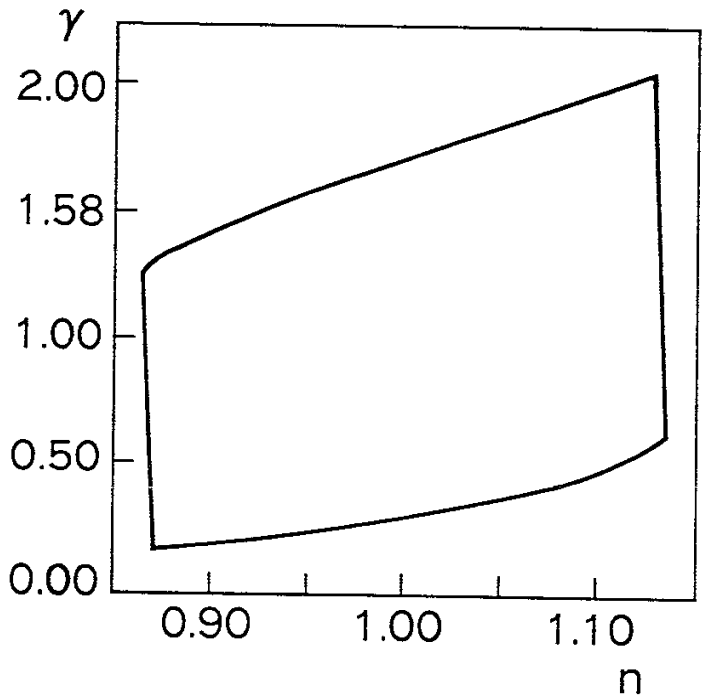

Fig. 4(c)

Fig. 5(a)

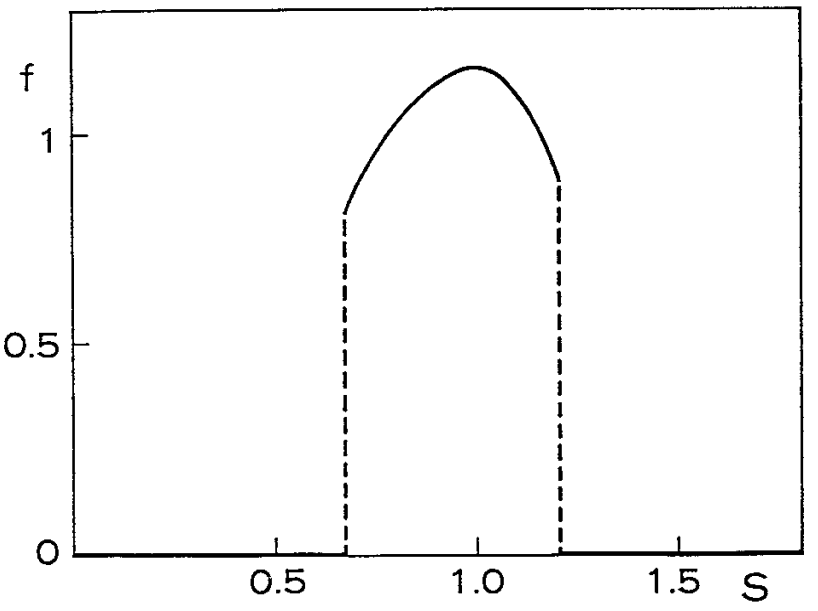

Fig. 5(b)

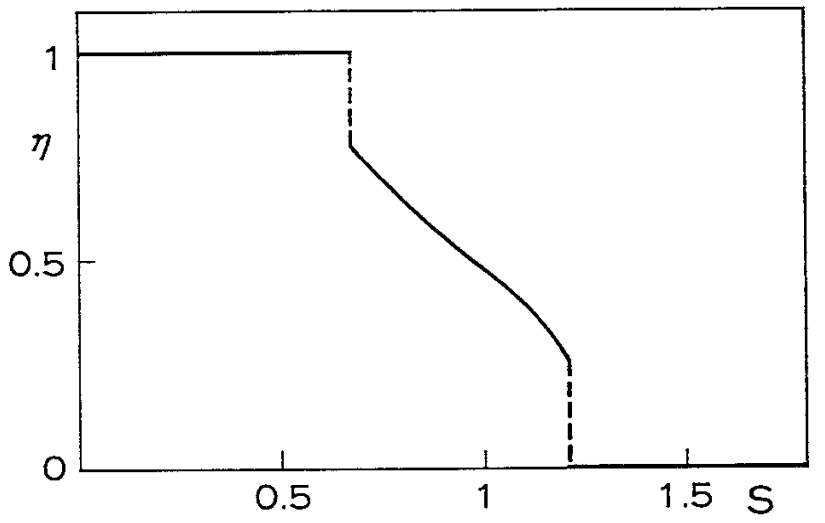

Fig. (6)

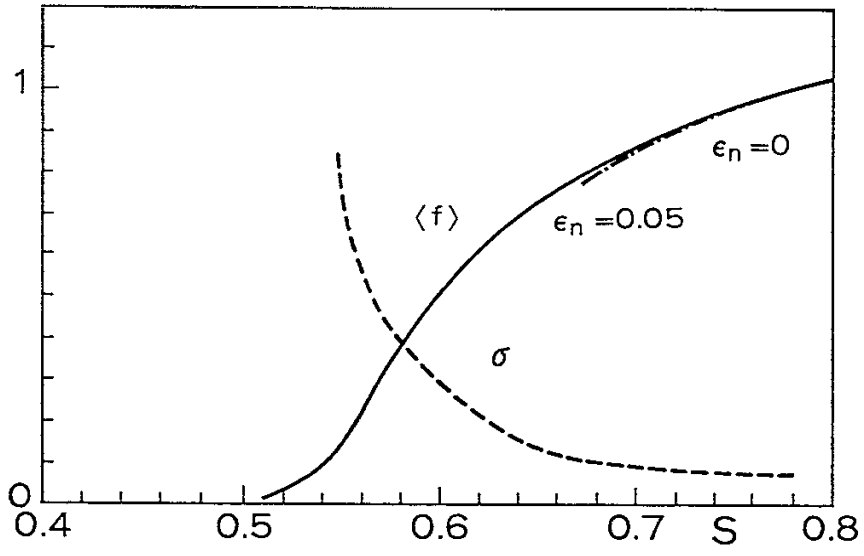

Fig. 7

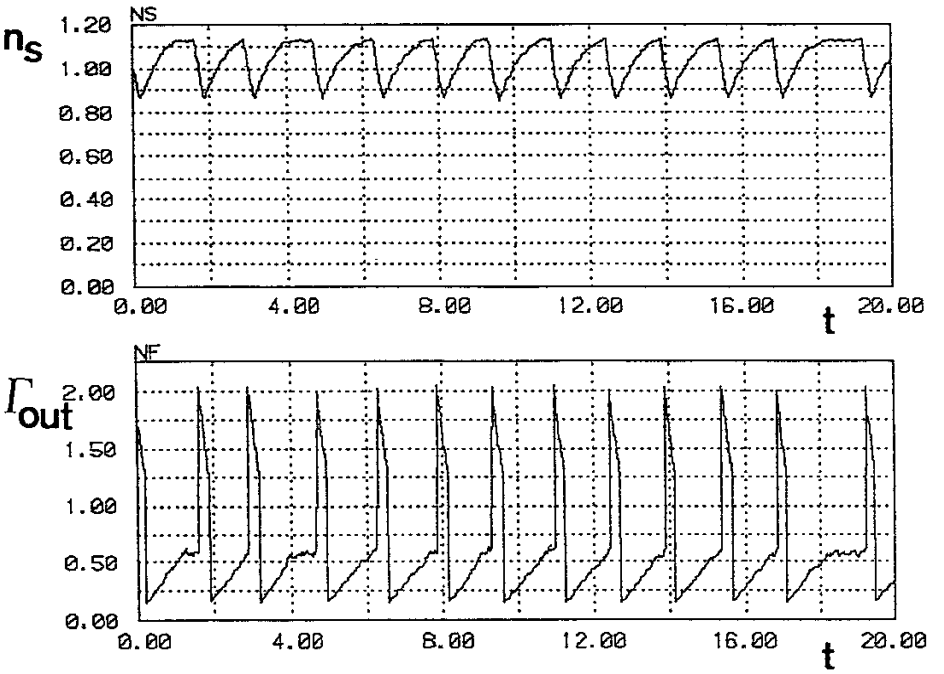
NS
n_s
1.20
1.00
0.80
0.60
0.40
0.20
0.00
0.00
4.00
8.00
12.00
16.00
20.00
t
NF
Γ_{out}
2.00
1.50
1.00
0.50
0.00
0.00
4.00
8.00
12.00
16.00
20.00
t

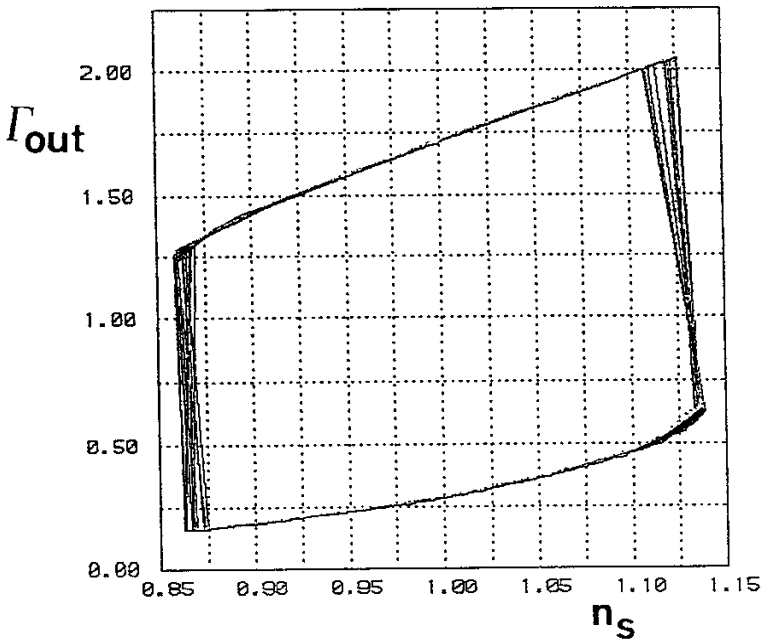
Γ_{out}
2.00
1.50
1.00
0.50
0.00
0.85
0.90
0.95
1.00
1.05
1.10
1.15
n_s

Fig.8(a)

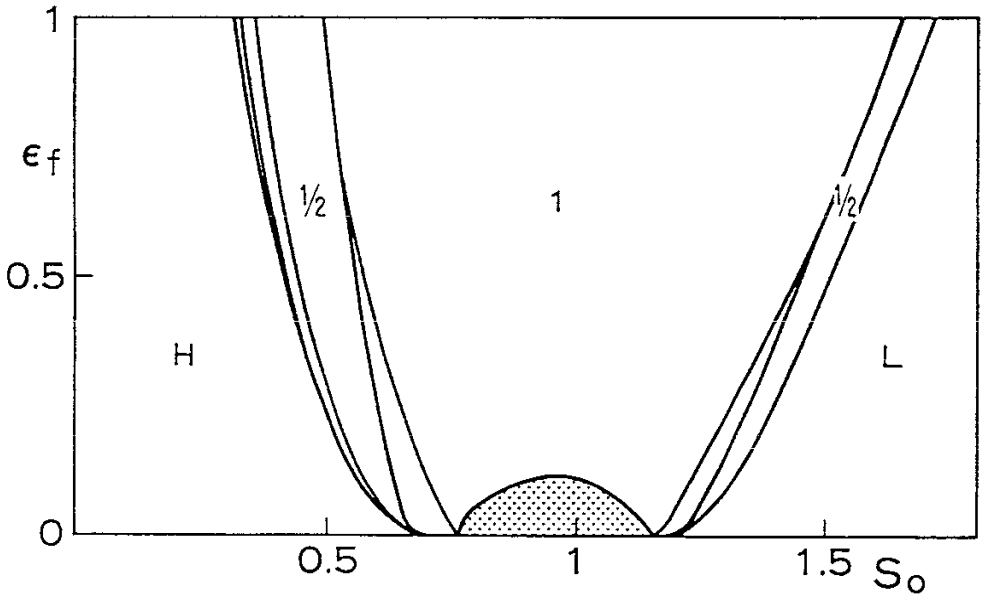
1
ϵ_f
0.5
0
H
1/2
1
1/2
L
0.5
1
1.5
S_o

Fig.8(b)

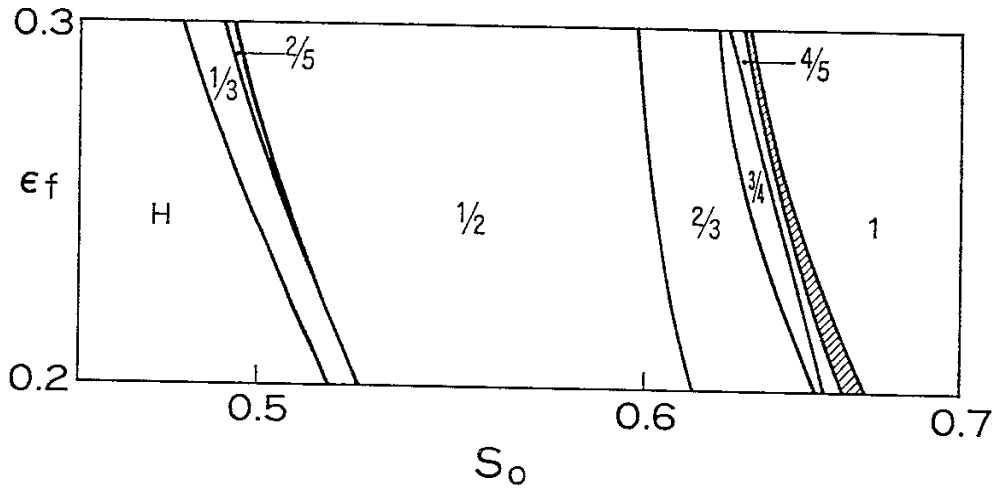
0.3
ϵ_f
0.2
H
1/3
2/5
1/2
2/3
3/4
4/5
1
0.5
0.6
0.7
S_o

Fig. 9

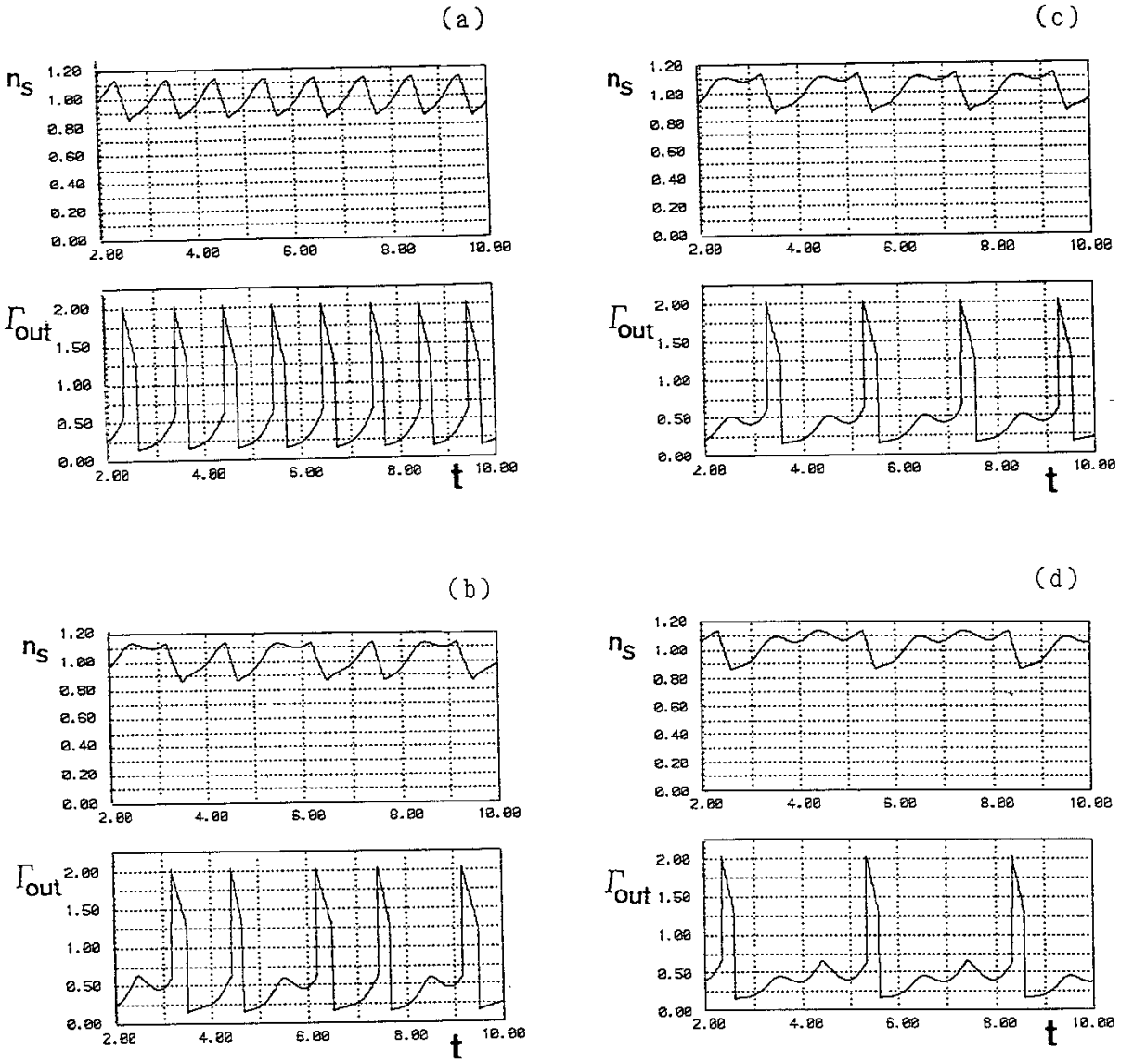
(a)
(c)
(b)
(d)
n_s
Γ_{out}
t
1.20
1.00
0.80
0.60
0.40
0.20
0.00
2.00
1.50
1.00
0.50
0.00
2.00
4.00
6.00
8.00
10.00

Fig. 10

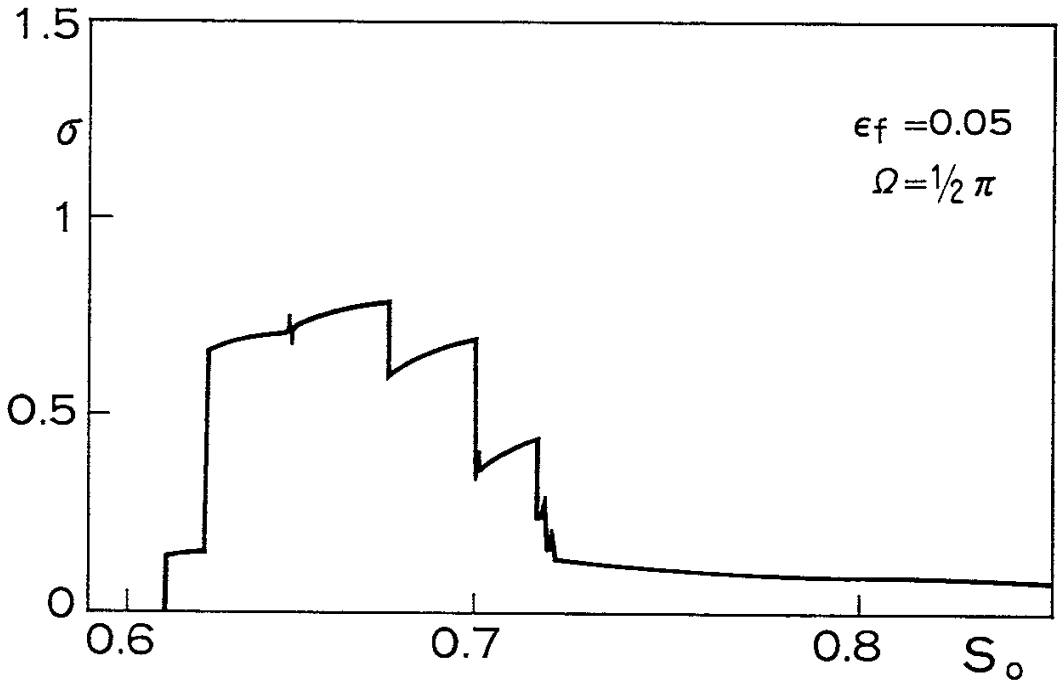

Fig. 11

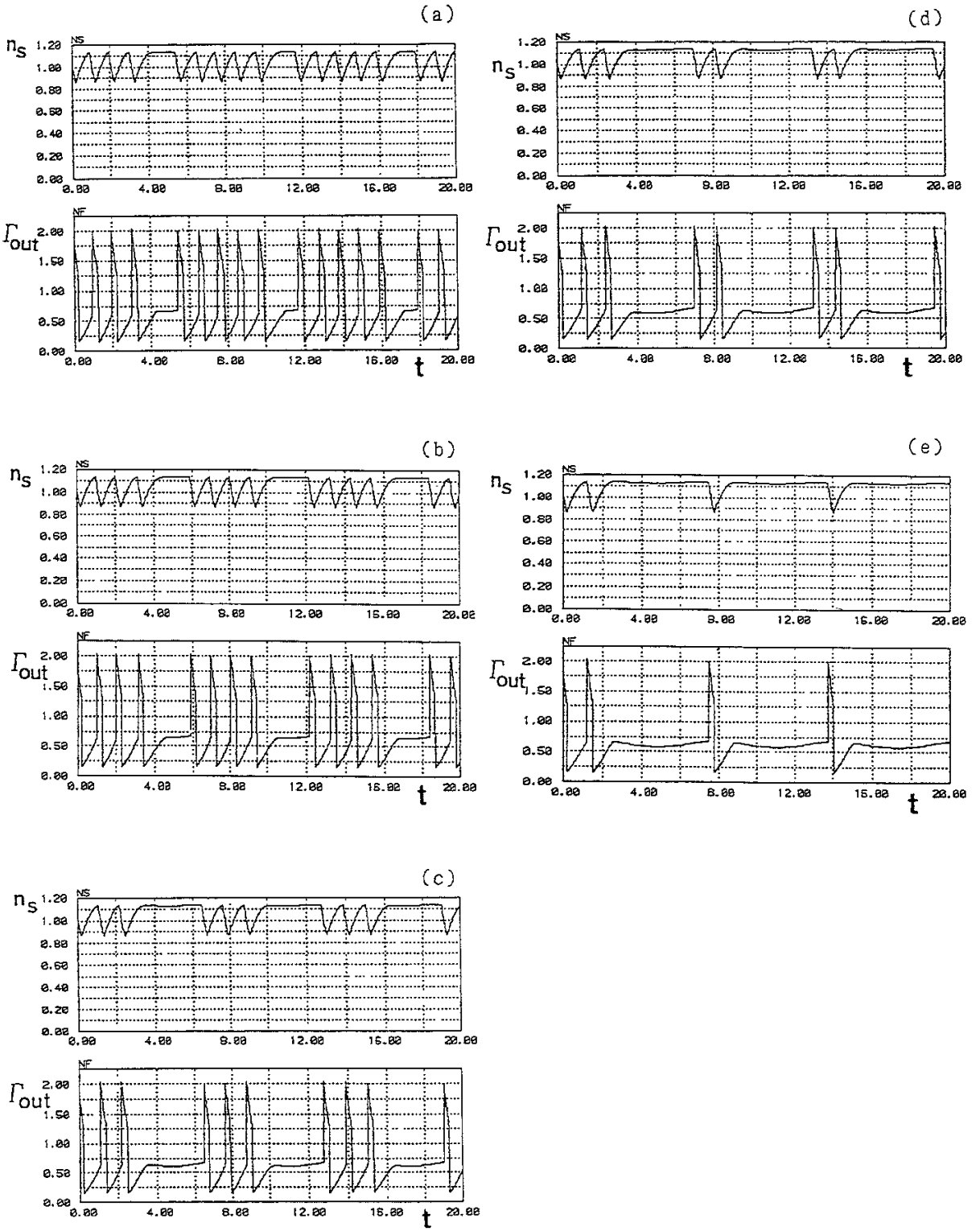

Fig. 12

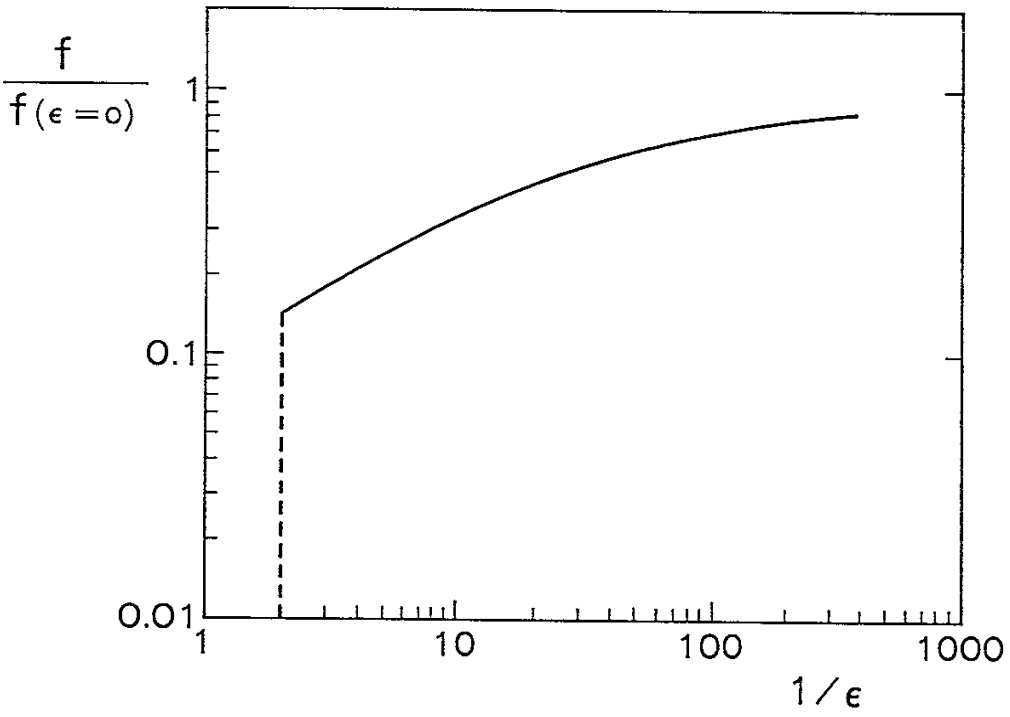

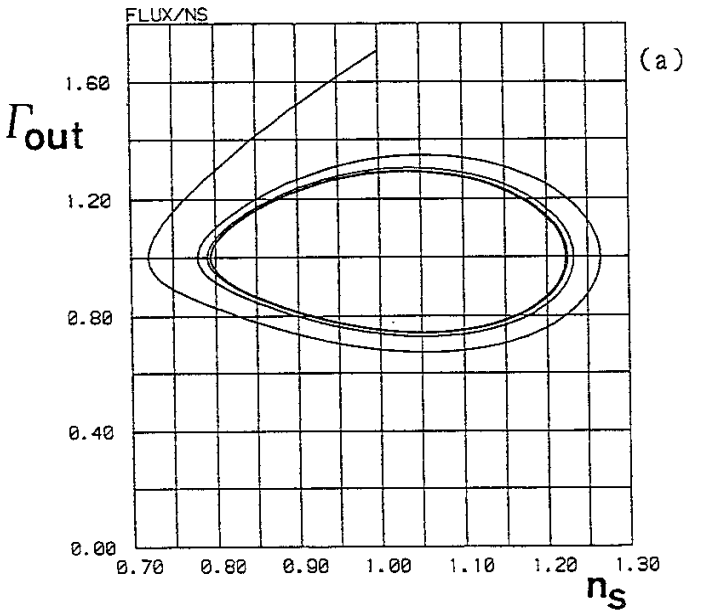
FLUX/NS
(a)
Γ_{out}
1.60
1.20
0.80
0.40
0.00
0.70
0.80
0.90
1.00
1.10
1.20
1.30
n_s

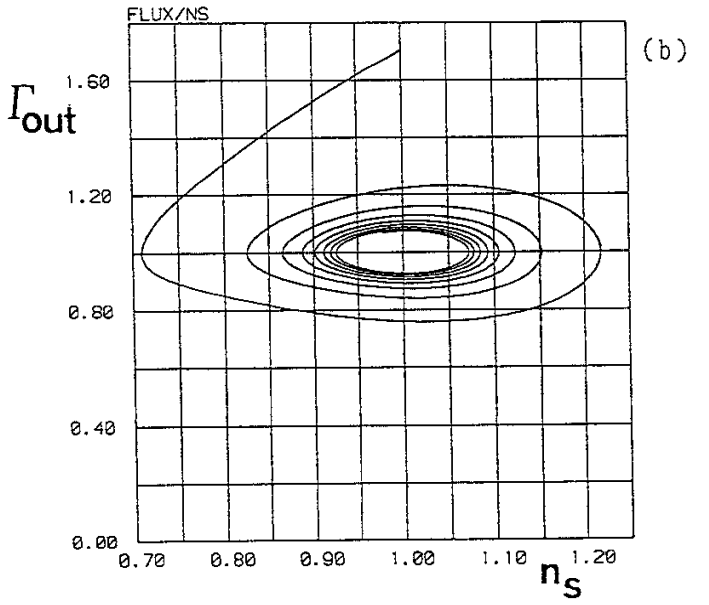
FLUX/NS
(b)
Γ_{out}
1.60
1.20
0.80
0.40
0.00
0.70
0.80
0.90
1.00
1.10
1.20
n_s

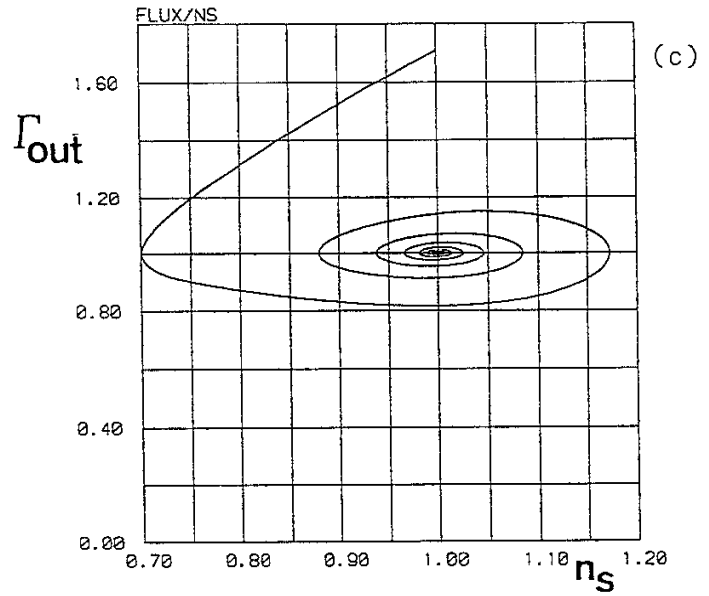
FLUX/NS
(c)
Γ_{out}
1.60
1.20
0.80
0.40
0.00
0.70
0.80
0.90
1.00
1.10
1.20
n_s

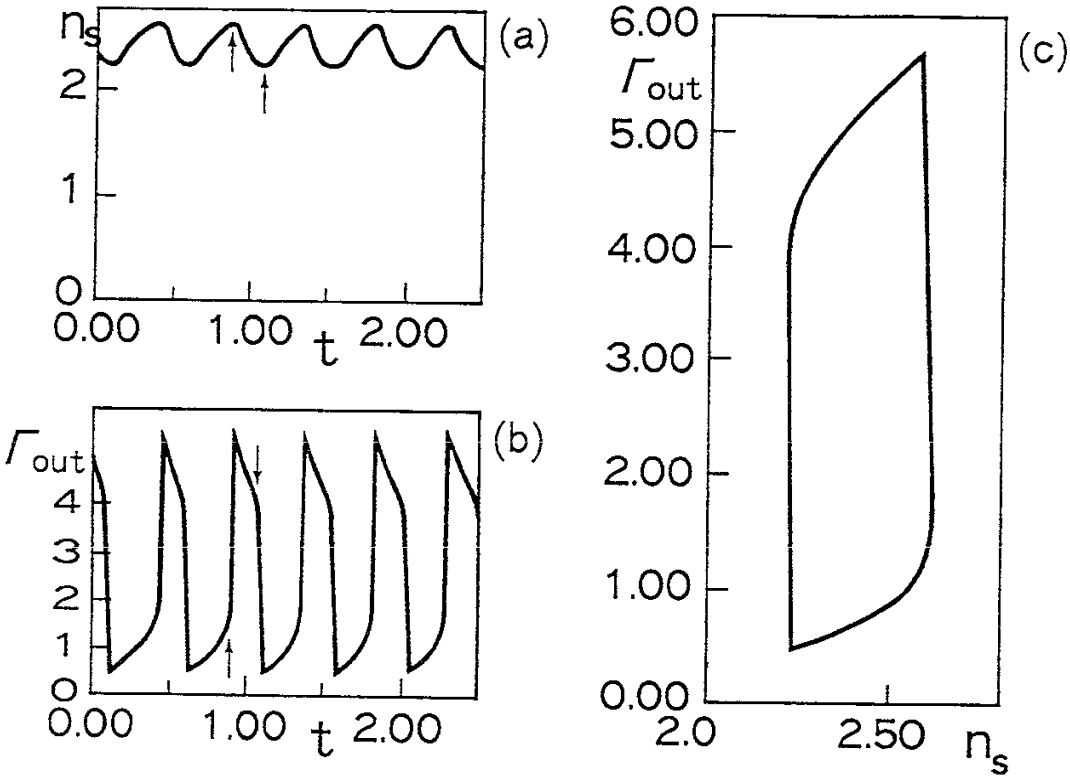
n_s
2
1
0
0.00
1.00
t
2.00
(a)
Γ_{out}
4
3
2
1
0
0.00
1.00
t
2.00
(b)
6.00
Γ_{out}
5.00
4.00
3.00
2.00
1.00
0.00
2.0
2.50
n_s
(c)

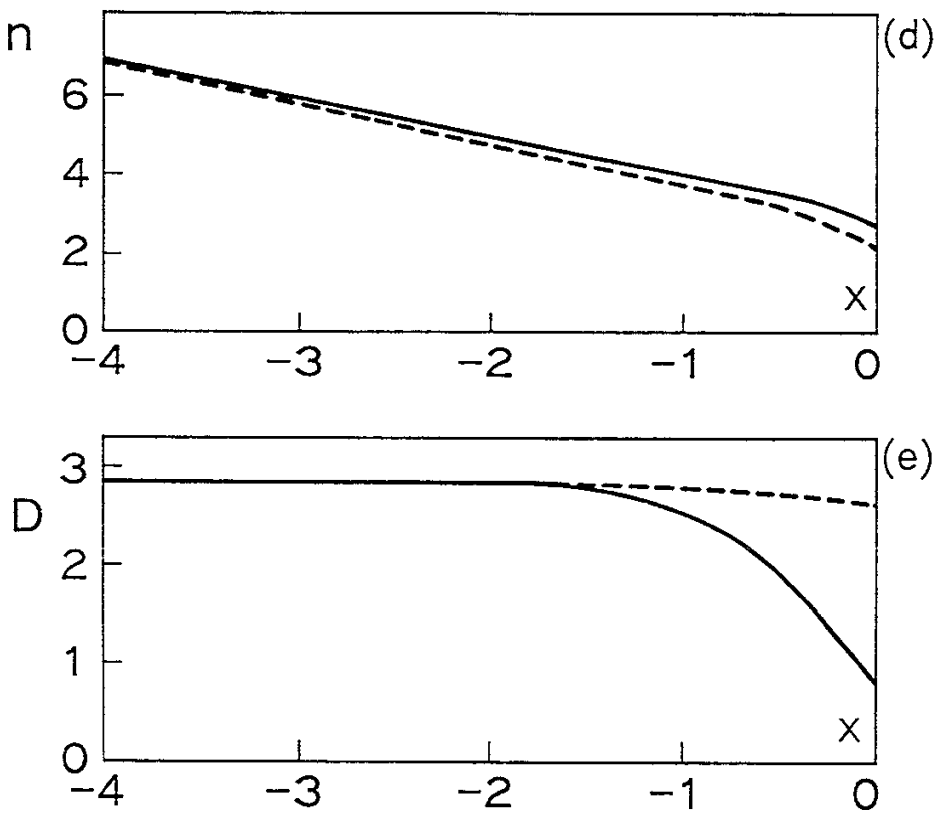
n
6
4
2
0
−4
−3
−2
−1
0
X
(d)
D
3
2
1
0
−4
−3
−2
−1
0
X
(e)

Fig. 14

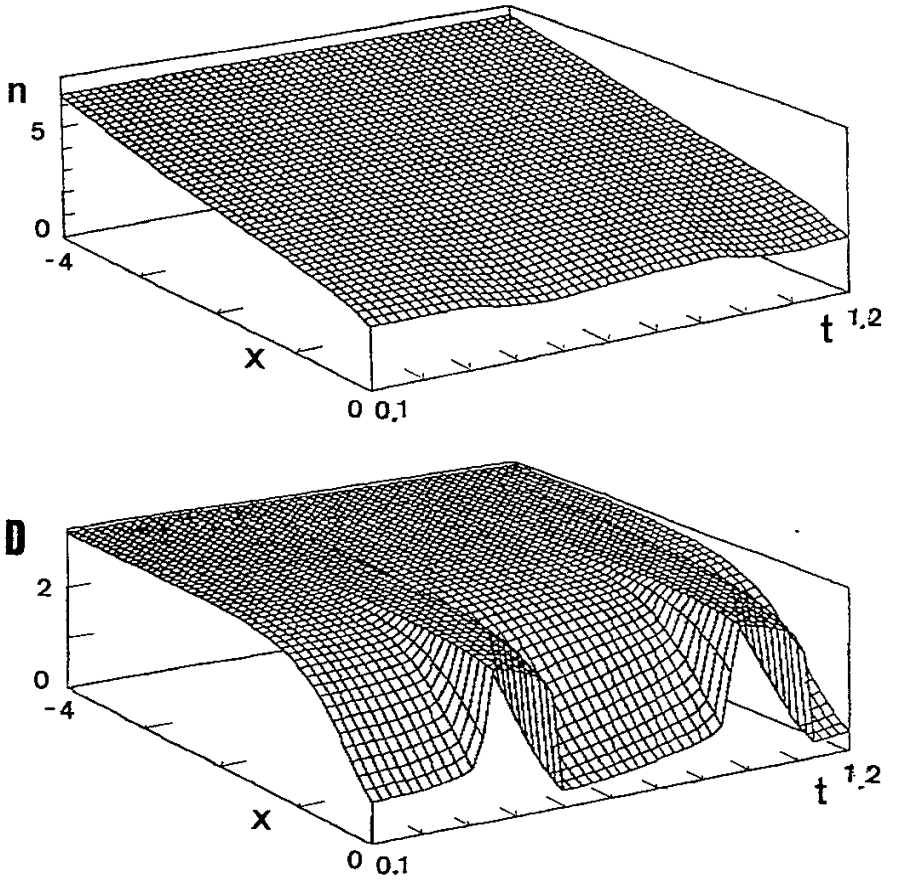

(f)

(g)

Fig. 15

(a)

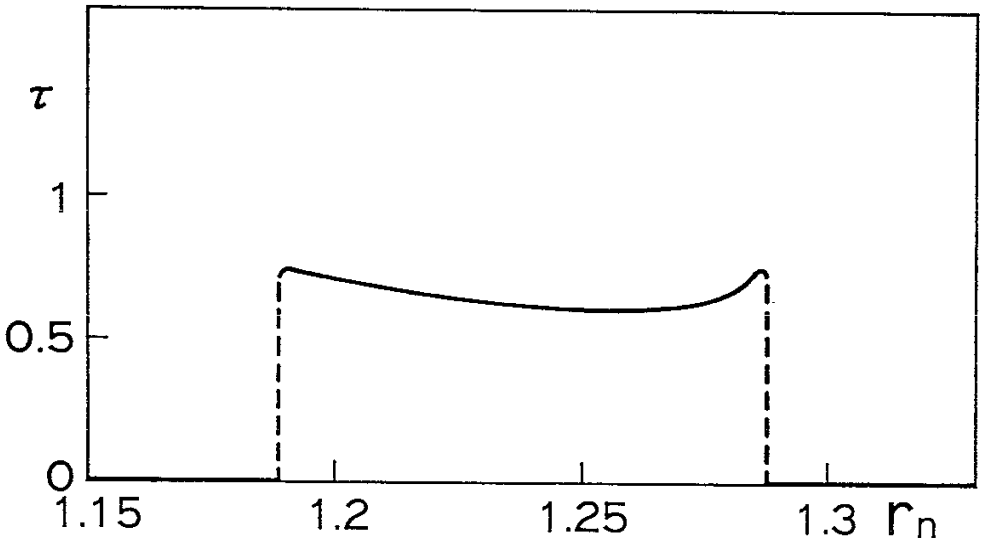

(b)

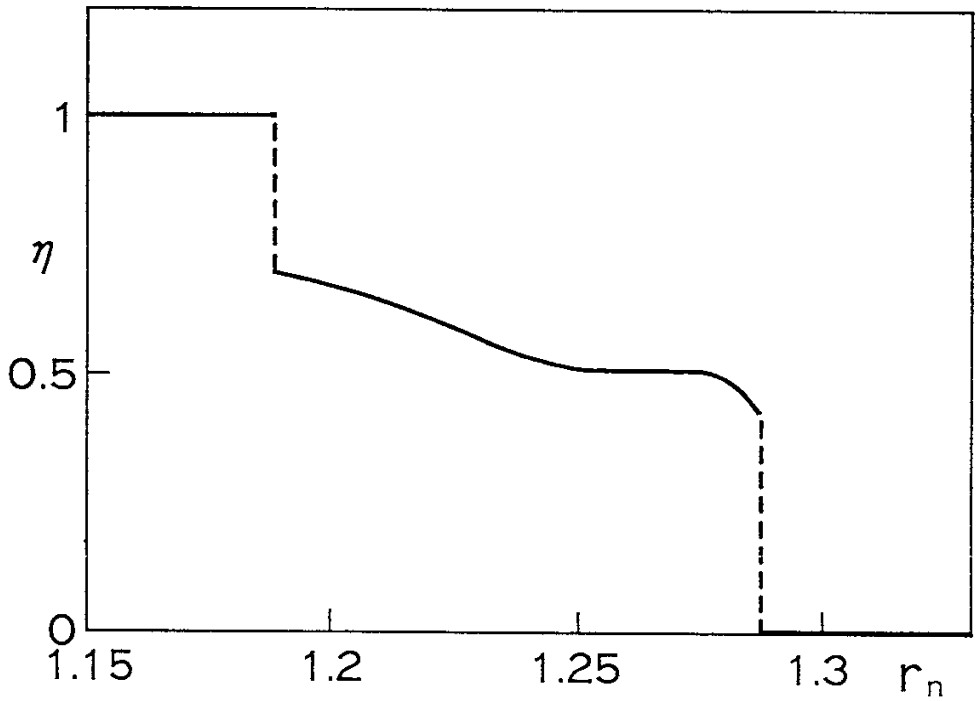

Fig. 16

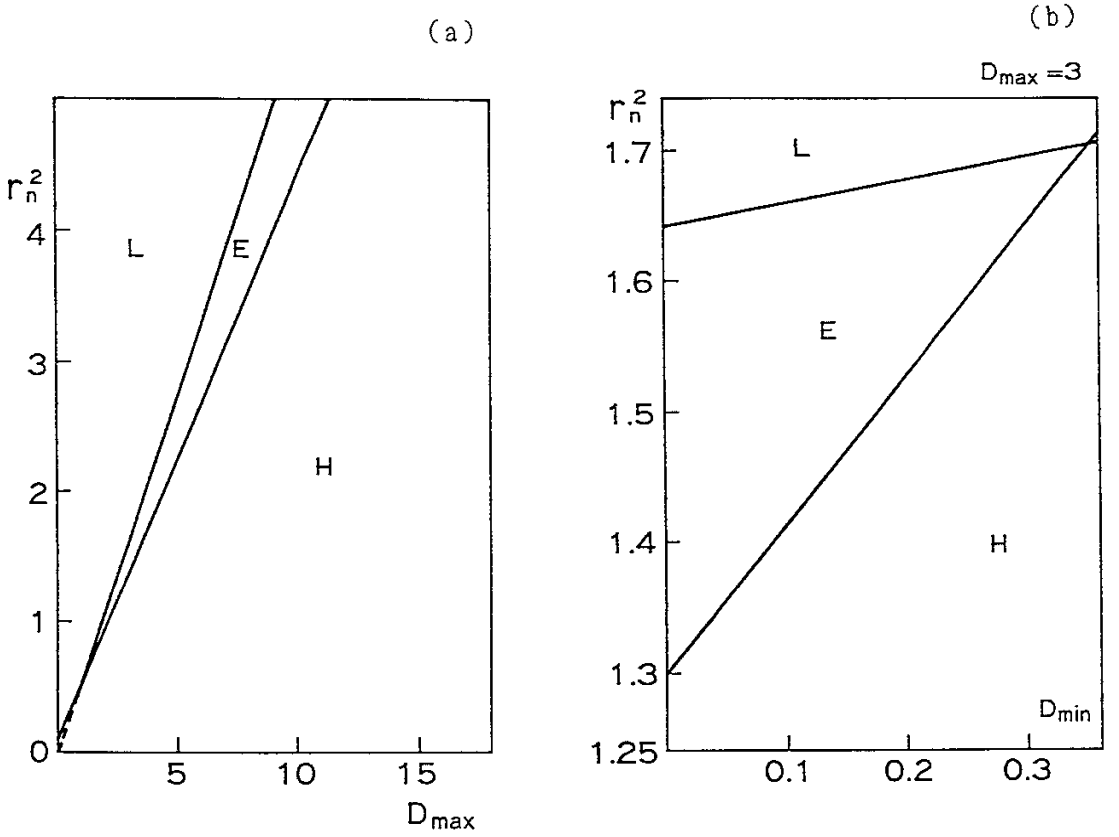
(a)
r_n^2
4
3
2
1
0
L
E
H
5
10
15
D_{max}
(b)
D_{max} =3
r_n^2
1.7
1.6
1.5
1.4
1.3
1.25
L
E
H
0.1
0.2
0.3
D_{min}

(a)

Fig. 17

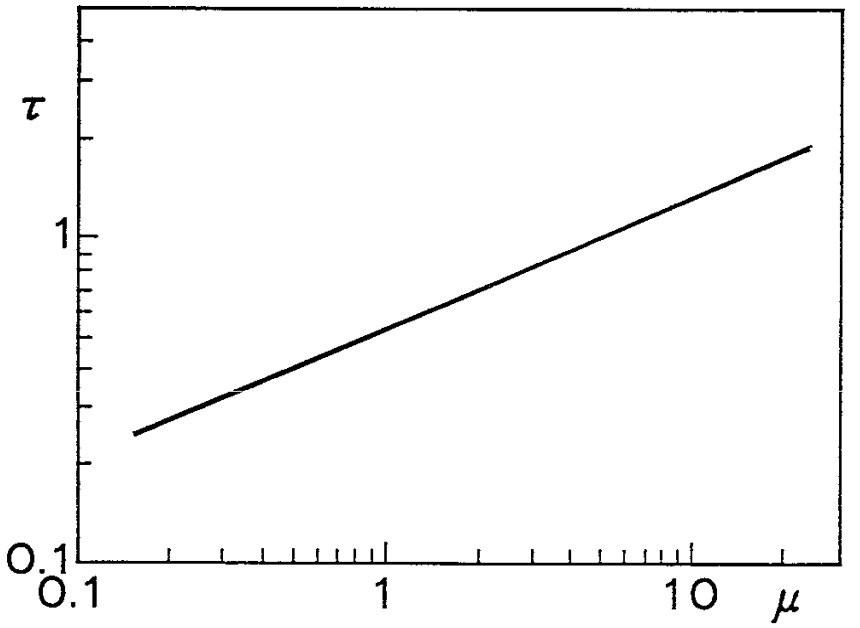

(b)

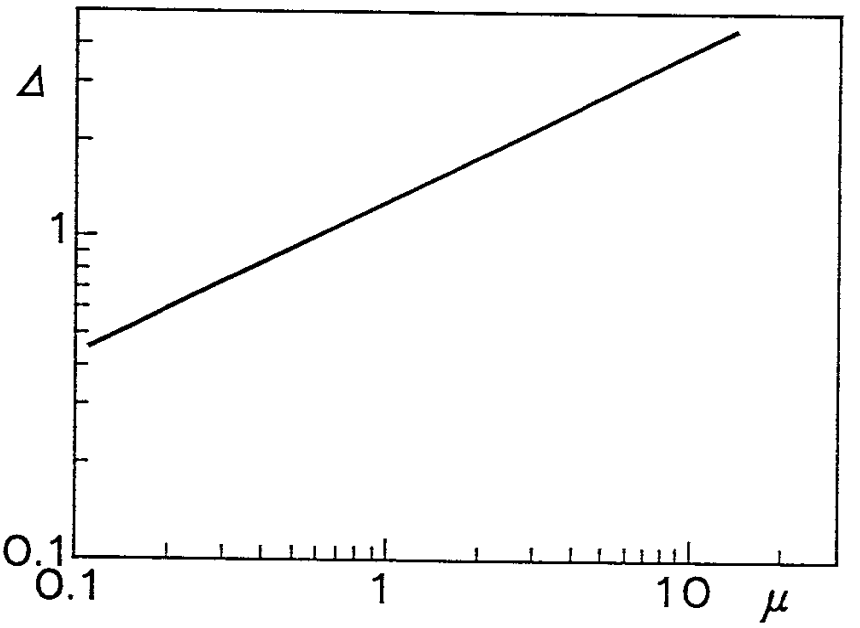

Fig. 18

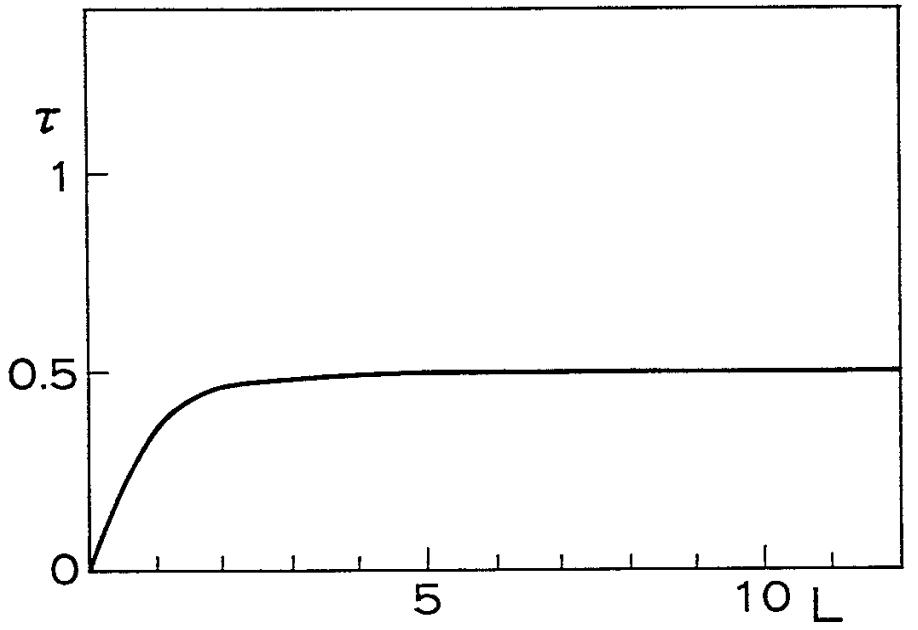

Fig. 19

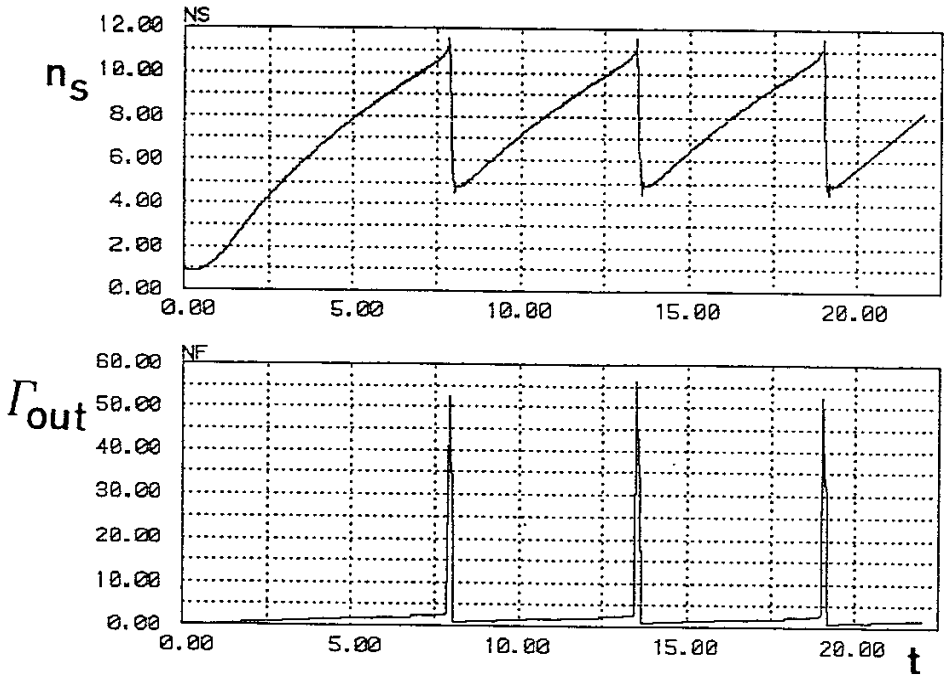
NS
12.00
10.00
8.00
6.00
4.00
2.00
0.00
n_s
0.00
5.00
10.00
15.00
20.00
NF
60.00
50.00
40.00
30.00
20.00
10.00
0.00
Γ_{out}
0.00
5.00
10.00
15.00
20.00
t

Fig. 20

(a)

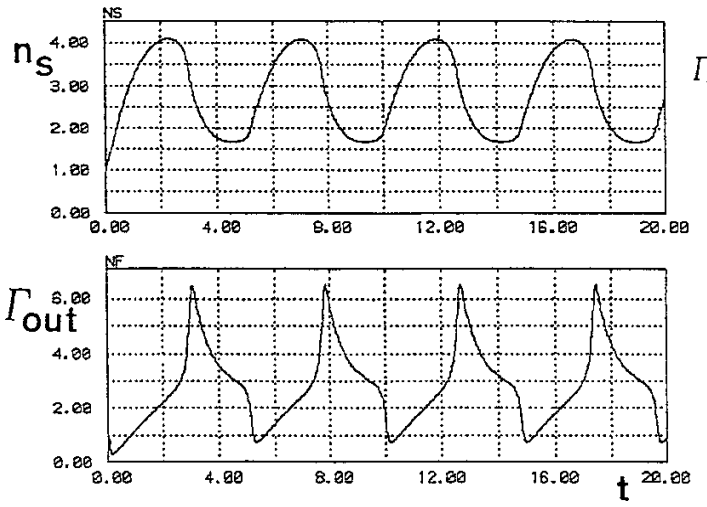
NS
n_s
4.00
3.00
2.00
1.00
0.00
0.00
4.00
8.00
12.00
16.00
20.00
NF
Γ_{out}
6.00
4.00
2.00
0.00
0.00
4.00
8.00
12.00
16.00
20.00
t

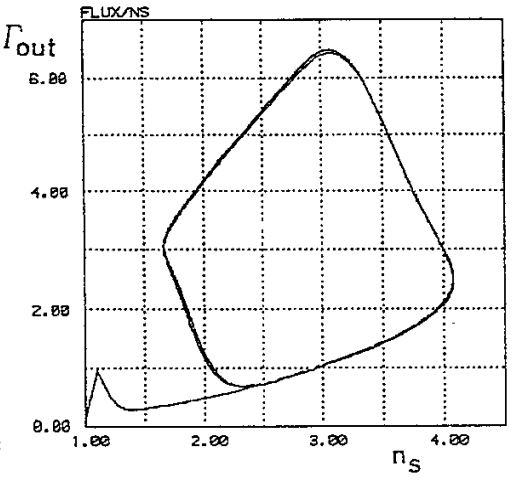
FLUX/NS
Γ_{out}
6.00
4.00
2.00
0.00
1.00
2.00
3.00
4.00
n_s

(b)

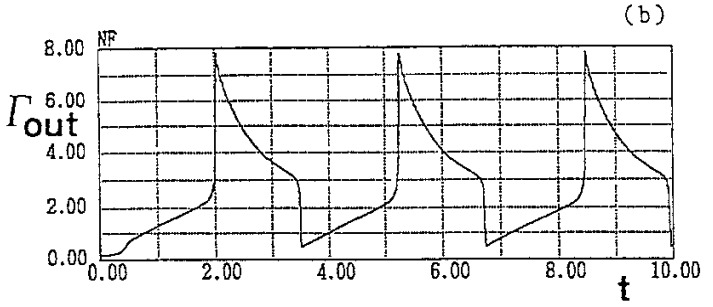
NF
Γ_{out}
8.00
6.00
4.00
2.00
0.00
0.00
2.00
4.00
6.00
8.00
10.00
t

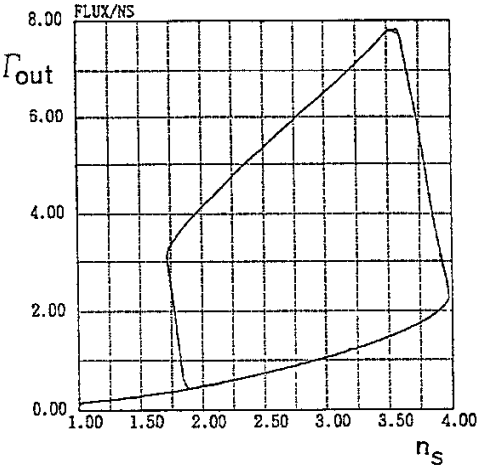
FLUX/NS
Γ_{out}
8.00
6.00
4.00
2.00
0.00
1.00
1.50
2.00
2.50
3.00
3.50
4.00
n_s

(c)

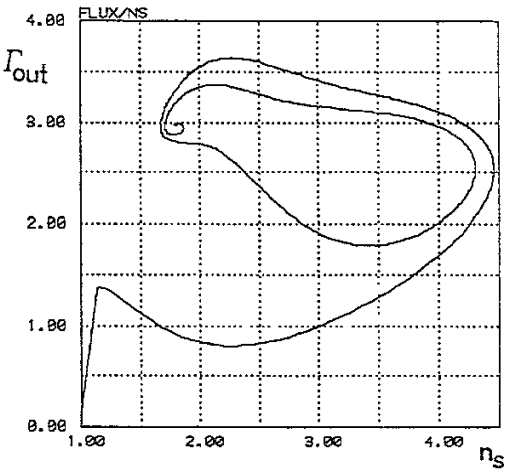
FLUX/NS
Γ_{out}
4.00
3.00
2.00
1.00
0.00
1.00
2.00
3.00
4.00
n_s

Fig. A1

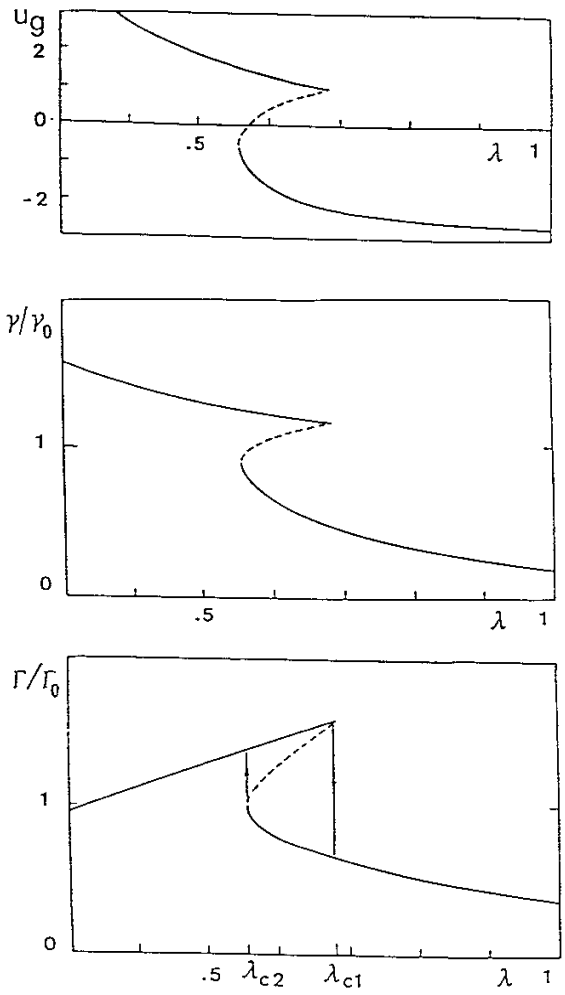

Fig. B1(a)

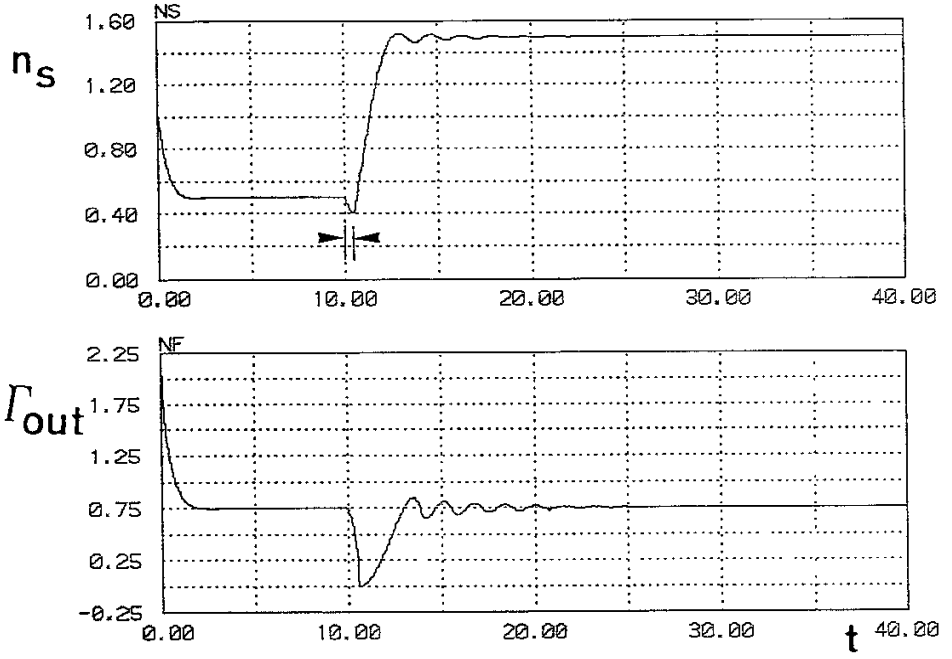
NS
n_s
1.60
1.20
0.80
0.40
0.00
0.00
10.00
20.00
30.00
40.00
NF
Γ_{out}
2.25
1.75
1.25
0.75
0.25
-0.25
0.00
10.00
20.00
30.00
t
40.00

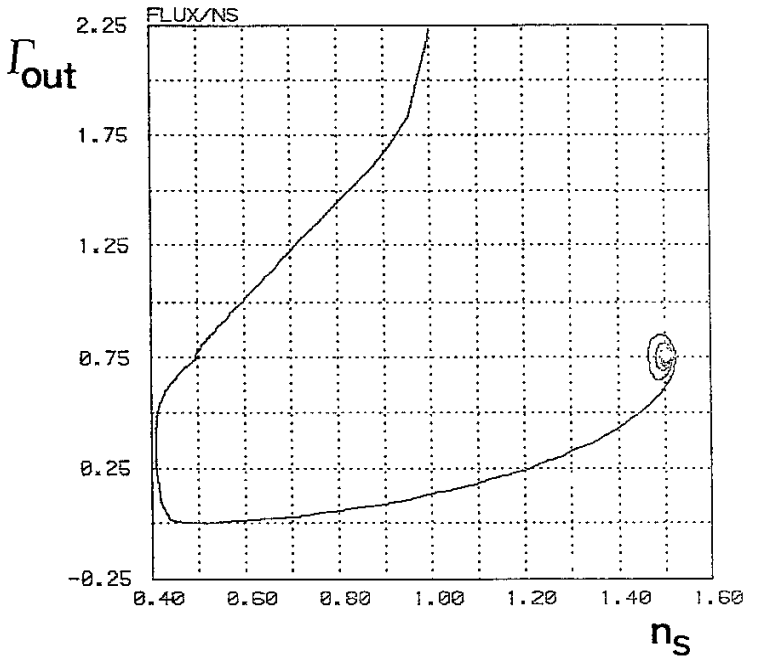
FLUX/NS
Γ_{out}
2.25
1.75
1.25
0.75
0.25
-0.25
0.40
0.60
0.80
1.00
1.20
1.40
1.60
n_s

Fig. B1(b)

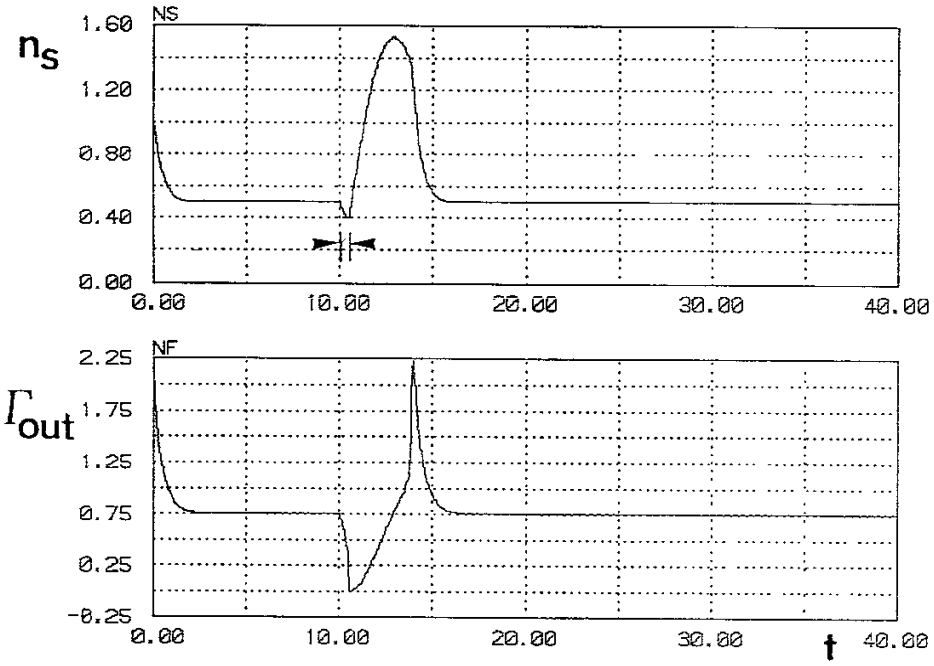
NS
n_s
1.60
1.20
0.80
0.40
0.00
0.00
10.00
20.00
30.00
40.00
NF
Γ_{out}
2.25
1.75
1.25
0.75
0.25
-0.25
0.00
10.00
20.00
30.00
t
40.00

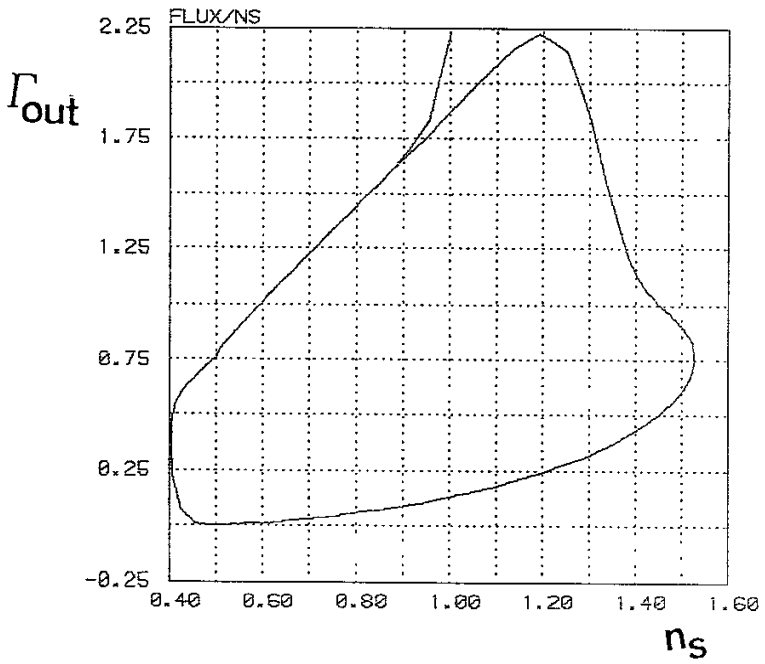
FLUX/NS
Γ_{out}
2.25
1.75
1.25
0.75
0.25
-0.25
0.40
0.60
0.80
1.00
1.20
1.40
1.60
n_s

Recent Issues of NIFS Series

NIFS-43 K.Yamazaki, N.Ohyabu, M.Okamoto, T.Amano, J.Todoroki, Y.Ogawa, N.Nakajima, H.Akao, M.Asao, J.Fujita, Y.Hamada, T.Hayashi, T.Kamimura, H.Kaneko, T.Kuroda, S.Morimoto, N.Noda, T.Obiki, H.Sanuki, T.Sato, T.Satow, M.Wakatani, T.Watanabe, J.Yamamoto, O.Motojima, M.Fujiwara, A.Iiyoshi and LHD Design Group, *Physics Studies on Helical Confinement Configurations with l=2 Continuous Coil Systems*; Sep. 1990

NIFS-44 T.Hayashi, A.Takei, N.Ohyabu, T.Sato, M.Wakatani, H.Sugama, M.Yagi, K.Watanabe, B.G.Hong and W.Horton, *Equilibrium Beta Limit and Anomalous Transport Studies of Helical Systems*; Sep. 1990

NIFS-45 R.Horiuchi, T.Sato, and M.Tanaka, *Three-Dimensional Particle Simulation Study on Stabilization of the FRC Tilting Instability*; Sep. 1990

NIFS-46 K.Kusano, T.Tamano and T. Sato, *Simulation Study of Nonlinear Dynamics in Reversed-Field Pinch Configuration*; Sep. 1990

NIFS-47 Yoshi H.Ichikawa, *Solitons and Chaos in Plasma*; Sep. 1990

NIFS-48 T.Seki, R.Kumazawa, Y.Takase, A.Fukuyama, T.Watari, A.Ando, Y.Oka, O.Kaneko, K.Adati, R.Akiyama, R.Ando, T.Aoki, Y.Hamada, S.Hidekuma, S.Hirokura, K.Ida, K.Itoh, S.-I.Itoh, E.Kako, A. Karita, K.Kawahata, T.Kawamoto, Y.Kawasumi, S.Kitagawa, Y.Kitoh, M.Kojima, T.Kuroda, K.Masai, S.Morita, K.Narihara, Y.Ogawa, K.Ohkubo, S.Okajima, T.Ozaki, M.Sakamoto, M.Sasao, K.Sato, K.N.Sato, F.Shinbo, H.Takahashi, S.Tanahashi, Y.Taniguchi, K.Toi and T.Tsuzuki, *Application of Intermediate Frequency Range Fast Wave to JIPP T-IIU Plasma*; Sep.1990

NIFS-49 A.Kageyama, K.Watanabe and T.Sato, *Global Simulation of the Magnetosphere with a Long Tail: The Formation and Ejection of Plasmoids*; Sep.1990

NIFS-50 S.Koide, *3-Dimensional Simulation of Dynamo Effect of Reversed Field Pinch*; Sep. 1990

NIFS-51 O.Motojima, K. Akaishi, M.Asao, K.Fujii, J.Fujita, T.Hino, Y.Hamada, H.Kaneko, S.Kitagawa, Y.Kubota, T.Kuroda, T.Mito, S.Morimoto, N.Noda, Y.Ogawa, I.Ohtake, N.Ohyabu, A.Sagara, T. Satow, K.Takahata, M.Takeo, S.Tanahashi, T.Tsuzuki, S.Yamada, J.Yamamoto, K.Yamazaki, N.Yanagi, H.Yonezu, M.Fujiwara, A.Iiyoshi and LHD Design Group, *Engineering Design Study of Superconducting Large Helical Device*; Sep. 1990

NIFS-52 T.Sato, R.Horiuchi, K. Watanabe, T. Hayashi and K.Kusano, *Self-Organizing Magnetohydrodynamic Plasma*; Sep. 1990

NIFS-53 M.Okamoto and N.Nakajima, *Bootstrap Currents in Stellarators and Tokamaks*; Sep. 1990

NIFS-54 K.Itoh and S.-I.Itoh, *Peaked-Density Profile Mode and Improved Confinement in Helical Systems*; Oct. 1990

NIFS-55 Y.Ueda, T.Enomoto and H.B.Stewart, *Chaotic Transients and Fractal Structures Governing Coupled Swing Dynamics*; Oct. 1990

NIFS-56 H.B.Stewart and Y.Ueda, *Catastrophes with Indeterminate Outcome*; Oct. 1990

NIFS-57 S.-I.Itoh, H.Maeda and Y.Miura, *Improved Modes and the Evaluation of Confinement Improvement*; Oct. 1990

NIFS-58 H.Maeda and S.-I.Itoh, *The Significance of Medium- or Small-size Devices in Fusion Research*; Oct. 1990

NIFS-59 A.Fukuyama, S.-I.Itoh, K.Itoh, K.Hamamatsu, V.S.Chan, S.C.Chiu, R.L.Miller and T.Ohkawa, *Nonresonant Current Drive by RF Helicity Injection*; Oct. 1990

NIFS-60 K.Ida, H.Yamada, H.Iguchi, S.Hidekuma, H.Sanuki, K.Yamazaki and CHS Group, *Electric Field Profile of CHS Heliotron/Torsatron Plasma with Tangential Neutral Beam Injection*; Oct. 1990

NIFS-61 T.Yabe and H.Hoshino, *Two- and Three-Dimensional Behavior of Rayleigh-Taylor and Kelvin-Helmholz Instabilities*; Oct. 1990

NIFS-62 H.B. Stewart, *Application of Fixed Point Theory to Chaotic Attractors of Forced Oscillators;* Nov. 1990

NIFS-63 K.Konn., M.Mituhashi, Yoshi H.Ichikawa,*Soliton on Thin Vortex Filament;* Dec. 1990

NIFS-64 K.Itoh, S.-I.Itoh and A.Fukuyama,*Impact of Improved Confinement on Fusion Research;* Dec. 1990

NIFS -65 A.Fukuyama, S.-I.Itoh and K. Itoh,*A Consistency Analysis on the Tokamak Reactor Plasmas;* Dec. 1990

NIFS-66 K.Itoh, H. Sanuki, S.-I. Itoh and K. Tani,*Effect of Radial Electric Field on α-Particle Loss in Tokamaks;* Dec. 1990

NIFS-67 K.Sato,and F.Miyawaki,*Effects of a Nonuniform Open Magnetic Field on the Plasma Presheath*; Jan.1991

NIFS-68 K.Itoh and S.-I.Itoh,*On Relation between Local Transport Coefficient and Global Confinement Scaling Law;* Jan. 1991

NIFS-69 T.Kato, K.Masai, T.Fujimoto,F.Koike, E.Källne, E.S.Marmar and J.E.Rice,*He-like Spectra Through Charge Exchange Processes in Tokamak Plasmas;* Jan.1991

NIFS-70 K. Ida, H. Yamada, H. Iguchi, K. Itoh and CHS Group, *Observation of Parallel Viscosity in the CHS Heliotron/Torsatron* ; Jan.1991

NIFS-71 H. Kaneko, *Spectral Analysis of the Heliotron Field with the Toroidal Harmonic Function in a Study of the Structure of Built-in Divertor* ; Jan. 1991

NIFS-72 S. -I. Itoh, H. Sanuki and K. Itoh, *Effect of Electric Field Inhomogeneities on Drift Wave Instabilities and Anomalous Transport* ; Jan. 1991

NIFS-73 Y.Nomura, Yoshi.H.Ichikawa and W.Horton, *Stabilities of Regular Motion in the Relativistic Standard Map*; Feb. 1991

NIFS-74 T.Yamagishi, *Electrostatic Drift Mode in Toroidal Plasma with Minority Energetic Particles,* Feb. 1991

NIFS-75 T.Yamagishi, *Effect of Energetic Particle Distribution on Bounce Resonance Excitation of the Ideal Ballooning Mode,* Feb. 1991

NIFS-76 T.Hayashi, A.Tadei, N.Ohyabu and T.Sato, *Suppression of Magnetic Surface Breading by Simple Extra Coils in Finite Beta Equilibrium of Helical System;* Feb. 1991

NIFS-77 N. Ohyabu, *High Temperature Divertor Plasma Operation*; Feb. 1991

NIFS-78 K.Kusano, T. Tamano and T. Sato, *Simulation Study of Toroidal Phase-Locking Mechanism in Reversed-Field Pinch Plasma*; Feb. 1991

NIFS-79 K. Nagasaki, K. Itoh and S. -I. Itoh, *Model of Divertor Biasing and Control of Scrape-off Layer and Divertor Plasmas*; Feb. 1991

NIFS-80 K. Nagasaki and K. Itoh, *Decay Process of a Magnetic Island by Forced Reconnection*; Mar. 1991

NIFS-81 K. Takahata, N. Yanagi, T. Mito, J. Yamamoto, O.Motojima and LHDDesign Group, K. Nakamoto, S. Mizukami, K. Kitamura, Y. Wachi, H. Shinohara, K. Yamamoto, M. Shibui, T. Uchida and K. Nakayama, *Design and Fabrication of Forced-Flow Coils as R&D Program for Large Helical Device*; Mar. 1991

NIFS-82 T. Aoki and T. Yabe, *Multi-dimensional Cubic Interpolation for ICF Hydrodynamics Simulation*; Apr. 1991

NIFS-83 K. Ida, S.-I. Itoh, K. Itoh, S. Hidekuma, Y. Miura, H. Kawashima, M. Mori, T. Matsuda, N. Suzuki, H. Tamai, T.Yamauchi and JFT-2M Group, *Density Peaking in the JFT-2M Tokamak Plasma with Counter Neutral Beam Injection* ; May 1991

NIFS-84 A. Iiyoshi, *Development of the Stellarator/Heliotron Research*; May 1991

NIFS-85 Y. Okabe, M. Sasao, H. Yamaoka, M. Wada and J. Fujita, *Dependence of Au^- Production upon the Target Work Function in a Plasma-Sputter-Type Negative Ion Source;* May 1991

NIFS-86 N. Nakajima and M. Okamoto, *Geometrical Effects of the Magnetic Field on the Neoclassical Flow, Current and Rotation in General Toroidal Systems*; May 1991

NIFS-87 S. -I. Itoh, K. Itoh, A. Fukuyama, Y. Miura and JFT-2M Group, *ELMy-H mode as Limit Cycle and Chaotic socillations in Tokamak Plasmas;* May 1991

NIFS-88 N.Matsunami and K.Kitoh, *High Resolution Spectroscopy of H^+ Energy Loss in Thin Carbon Film;* May 1991

NIFS-89 H. Sugama, N. Nakajima and M.Wakatani, *Nonlinear Behavior of Multiple-Helicity Resistive Interchange Modes near Marginally Stable States;* May 1991

NIFS-90 H. Hojo and T.Hatori, *Radial Transport Induced by Rotating RF Fields and Breakdown of Intrinsic Ambipolarity in a Magnetic Mirror*; May 1991

NIFS-91 M. Tanaka, S. Murakami, H. Takamaru and T.Sato, *Macroscale Implicit, Electromagnetic Particle Simulation of Inhomogeneous and Magnetized Plasmas in Multi-Dimensions;* May 1991

NIFS-92 S. - I. Itoh, *H-mode Physics, -Experimental Observations and Model Theories-, Lecture Notes, Spring College on Plasma Physics, May 27 - June 21 1991 at International Centre for Theoretical Physics (IAEA UNESCO) Trieste, Italy ;* Jun. 1991

NIFS-93 Y. Miura, K. Itoh, S. - I. Itoh, T. Takizuka, H. Tamai, T. Matsuda, N. Suzuki, M. Mori, H. Maeda and O. Kardaun, *Geometric Dependence of the Scaling Law on the Energy Confinement Time in H-mode Discharges;* Jun. 1991

NIFS-94 H. Sanuki, K. Itoh, K. Ida and S. - I. Itoh, *On Radial Electric Field Structure in CHS Torsatron / Heliotron;* Jun. 1991

NIFS-95 K. Itoh, H. Sanuki and S. - I. Itoh, *Influence of Fast Ion Loss on Radial Electric Field in Wendelstein VII-A Stellarator;* Jun. 1991